L2A+

Enhanced Aeolus L2A for depolarizing targets and impact on aerosol research and NWP

-

L2A+ Product Validation

Deliverable Item 04
[DI04]
(Final Version - FV)

Submitted to: Edward Malina (ESA)

	Name	Function	Date
Prepared by:	E. Proestakis	WP1000 – NOA	11/2024
	K. Rizos	WP3000 – NOA	11/2024
	A. Georgiou	WP4000 – NOA	11/2024
	A. A. Floutsi	WP2000 – TROPOS	11/2024
	H. Baars	WP2000 – Co-I – TROPOS	11/2024
Approved by:	V. Amiridis	PI	11/2024

-

National Observatory of Athens (NOA)
Institute for Astronomy, Astrophysics, Space Applications & Remote Sensing (IAASARS)
Vas. Pavlou & I. Metaxa, 15236 Penteli, Greece
&
Leibniz Institute for Tropospheric Research (TROPOS), Leipzig, Germany
&
European Centre for Medium-Range Weather Forecasts
[ECMWF]
Reading, United Kingdom

[This page is intentionally left blank.]

Table of Contents

1. ESA-L2A+ DI04 – Overview.

This document consists the Deliverable Item 04 (DI04) – Final Version (FV) submitted to the European Space Agency (ESA) by the consortium of the project "Enhanced Aeolus L2A for depolarizing targets and impact on aerosol research and NWP" (L2A+). DI04– "L2A+ product Validation" reports on activities and developments related to L2A+ Work Package 3 (WP3000) – "Development of the L2A+ aerosol product". More specifically, – "L2A+ product Validation" aims to document on the validation activities carried out for the comparisons of L2A+ with reference measurements in Cabo Verde from the ESA ASKOS campaign.

2. Introduction.

Central objective of the ESA L2A+ project consists the development of a refined Aeolus aerosol optical product (L2A+), based on AEL-FM/AEL-PRO algorithms, geostationary products, CAMS, and new CALIOP retrievals from the CALIPSO. Accordingly, the project aims to thoroughly compare the enhanced L2A+ product against L2A and validate against quality-assured measurements from the ASKOS/JATAC experiment in Cabo Verde, as described in the framework of L2A+ Work Package 3 (WP3000) – "Development of the L2A+ aerosol product" (Fig.2.1).

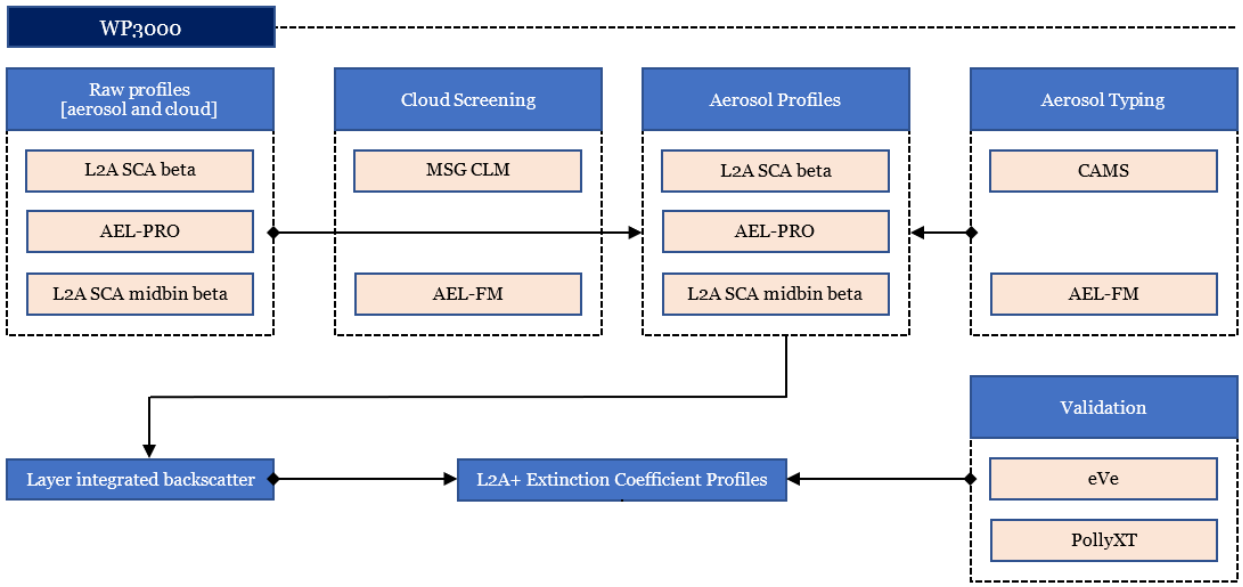

Figure 2.1: A graphical presentation of the WP3000 processing steps.

More specifically, a central DI04 objective is to use the available dataset from the ASKOS campaign for the evaluation and validation of the L2A+ product. The ASKOS 2021 operations constituted the ground-based component of the JATAC that was organised by ESA and the National Aeronautics and Space Administration (NASA) and was held at the tropical islands of Cabo Verde in July and September 2021. The main aim of JATAC was to provide quality-assured reference measurements for the validation of the products of the ESA-Aeolus satellite mission. ASKOS has been held in Mindelo on the island of Sao Vicente in Cape Verde deploying advanced active and passive remote sensing instrumentation such as a series of different lidar systems (e.g. eVe lidar, PollyXT lidar). As such, the ASKOS dataset contains measurements of the aerosol optical and physical properties. The collected ASKOS dataset are further enriched with additional measurements conducted during the

ASKOS 2022 operations at Mindelo, Cape Verde during summer 2022. The deployed instruments are presented in Fig.2.3.

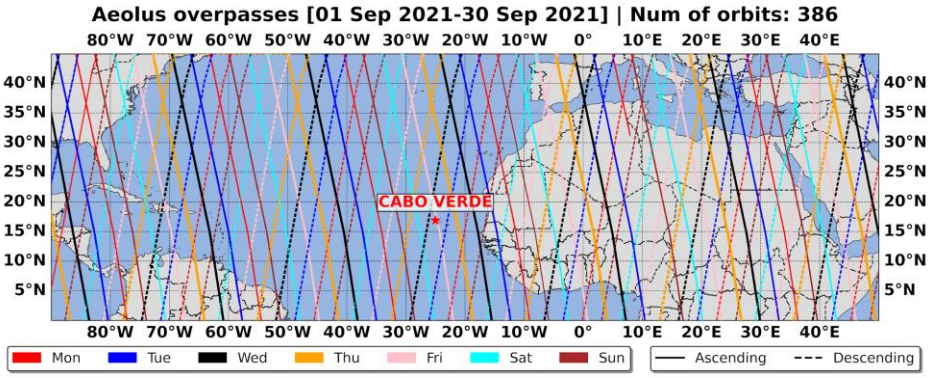

Figure 2.2: L2A+ Region of Interest (RoI).

Figure 2.3: The ground-based remote sensing instrumentation installed at the OSCM premises for the ESA-ASKOS experiment.

3. Horizontal homogeneity.

To assess the three-dimensional (3D) aerosol structure over Mindelo (OSCM) and establish the condition of robust validation intercomparison between the ground-based and satellite-based lidar system, it is important to have homogeneity in the cases of study. We implemented synergistically passive observations of the A-Train constellation of satellites, and to be more specific based on Aqua-MODIS and CALIOP-CALIPSO. This assessment is performed for the aerosol loading conditions expected at the Cape Verde/Mindelo ASKOS campaign site.

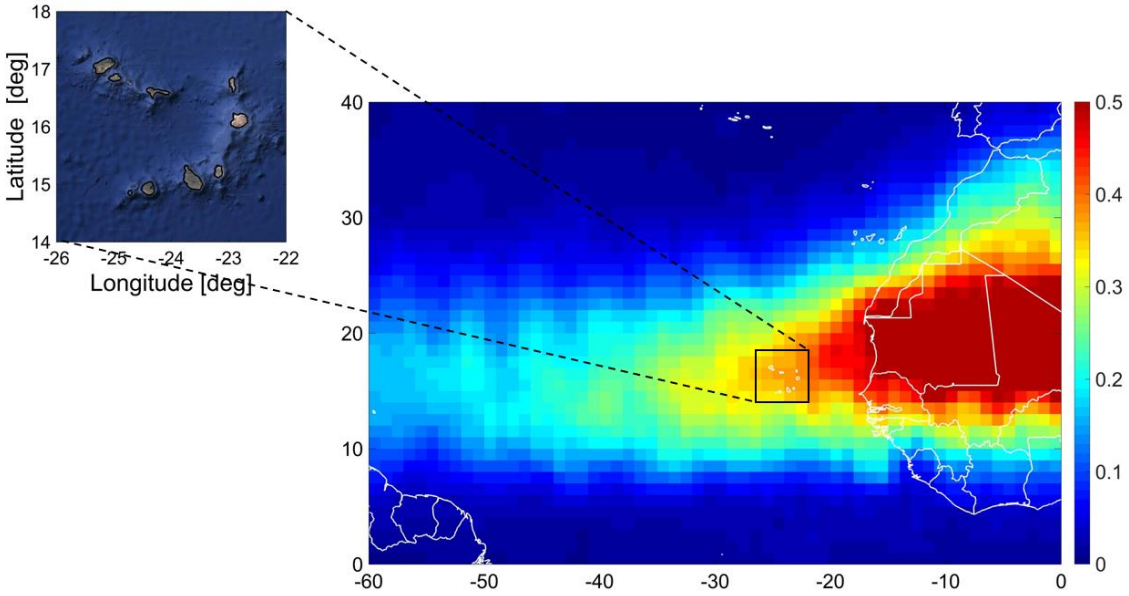

Figure 3.1: CALIPSO CALIOP DOD at 532 nm over Cape Verde in 1°x1° grid resolution for the period 2007-2015.

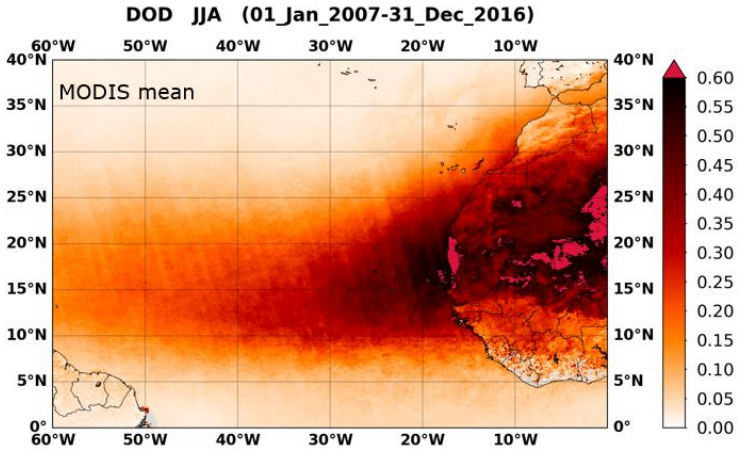

Figure 3.2: MODIS-Aqua (Level 2, Collection 6.1), for 2003 – 2019 dust climatology of Saharan Dust outflow (Gkikas et al., 2021).

- The Data used for the horizontal representativeness are as follows:
- MODIS – Aqua (Level 2, Collection 6.1).
- Spatial resolution: 10 km x 10 km (nadir view).
- Season: June – July – August (JJA).

- Temporal availability: 2003 – 2019 (17 years).
- Merged (DT and DB) AOD product.
- Consideration only of best (QA=3) AOD retrievals.
- Spatial averaging of AOD for 10 concentric circles with radii spanning from 10 to 100 km with an increasing step equal to 10 km.

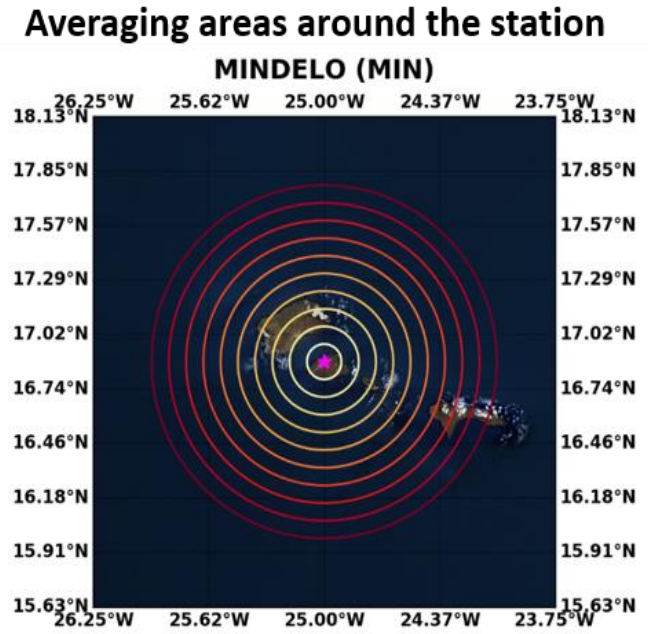

Figure 3.3: Averaging areas around the ESA-ASKOS domain.

- No-concurrent: Spatial averages are calculated regardless the AOD availability among the defined circles.
- Concurrent: Spatial averages are calculated only when AOD observations are simultaneously available in all defined circle areas (i.e., AODs are available in the inner circle-10km radius).
- The spatial averages are calculated within a circle centered at station coordinates and not in separate sections (i.e., ≤ 10km, 10-20km, …, 90-100km).

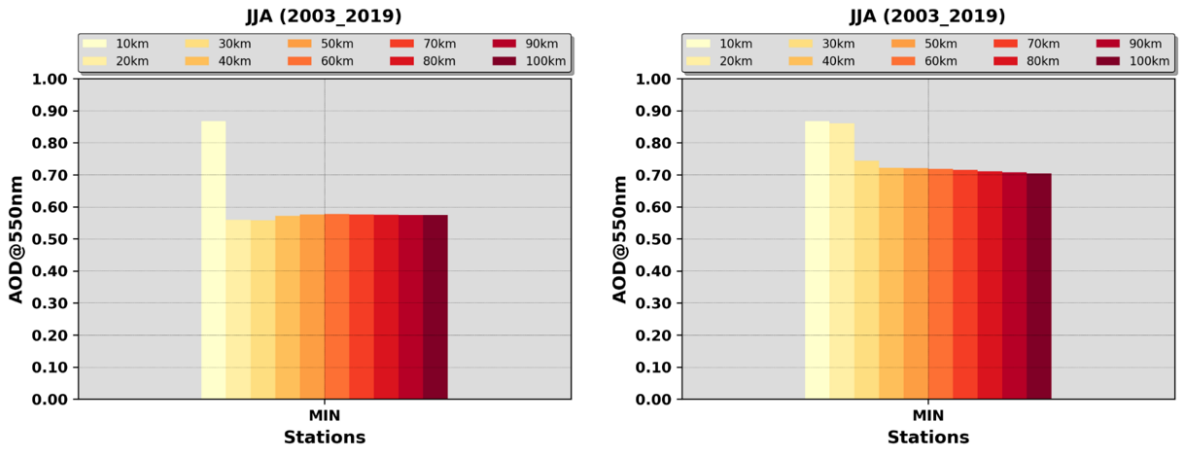

Figure 3.4: Spatial averages are calculated only when AOD observations are simultaneously available in all defined circle areas (i.e., AODs are available in the inner circle-10km radius), (a) non-concurrent and (b) concurrent approach.

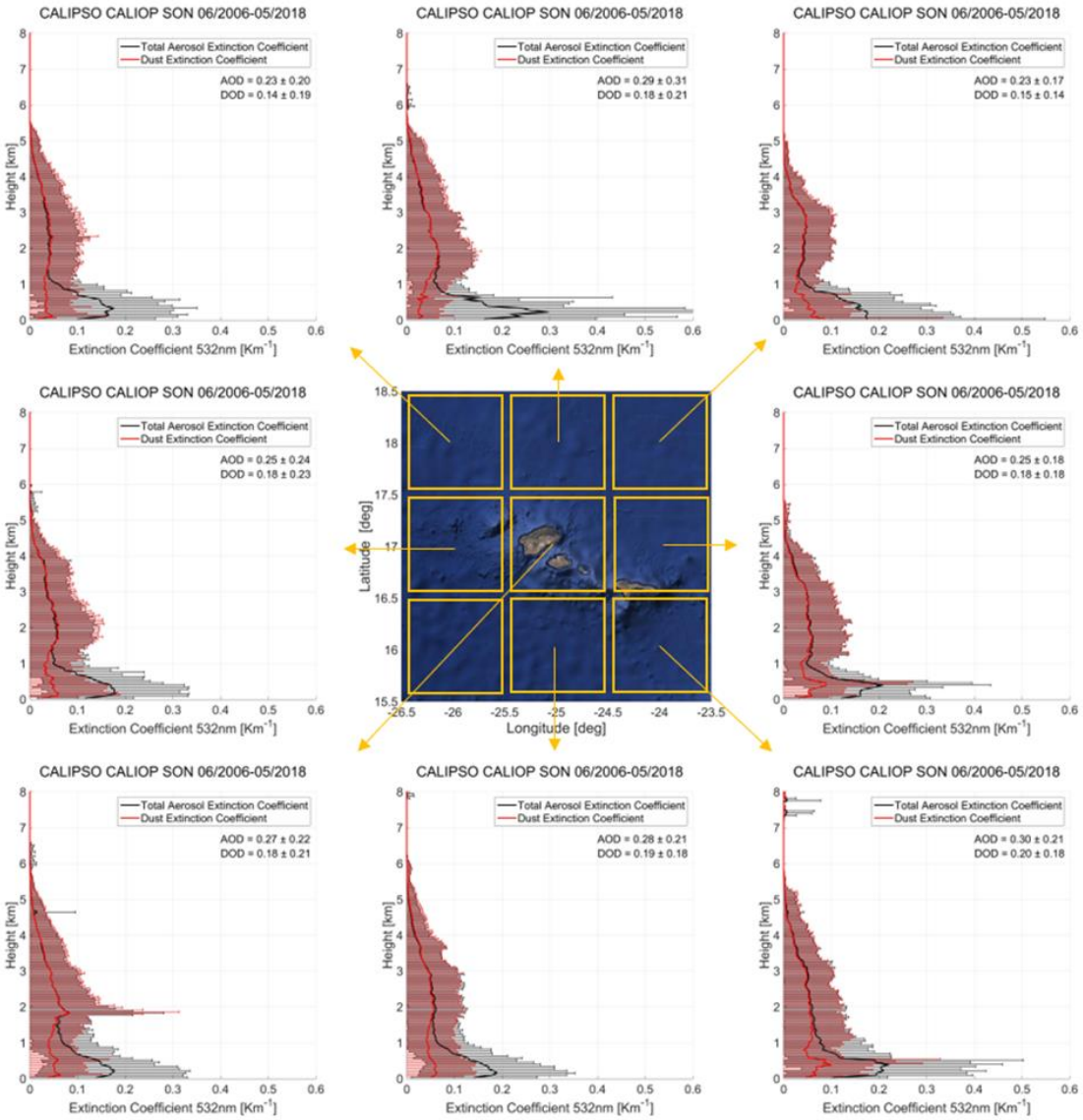

Figure 3.5: CALIPSO Cloud-Free L2 mean total aerosol extinction coefficient at 532 nm and pure-dust extinction coefficient at 532 nm, in a L3-equivalent grid of 10×10 grid spatial resolution for SON 2006-2018.

The results demonstrate the high spatial homogeneity in terms of aerosols in the ESA-ASKOS campaign proximity, allowing intercomparison and validation activities of ground-based and satellite-based aerosol profiles and products to be conducted.

4. ASKOS core instrumentation towards validation of the L2A+ products.

4.1. eVe lidar.

The eVe lidar operated by NOA is the ESA's ground reference system for the Aeolus L2A products validation since it is specifically designed and manufactured by Raymetrics S.A. to provide the Aeolus mission with ground reference measurements of the aerosols and clouds optical properties.

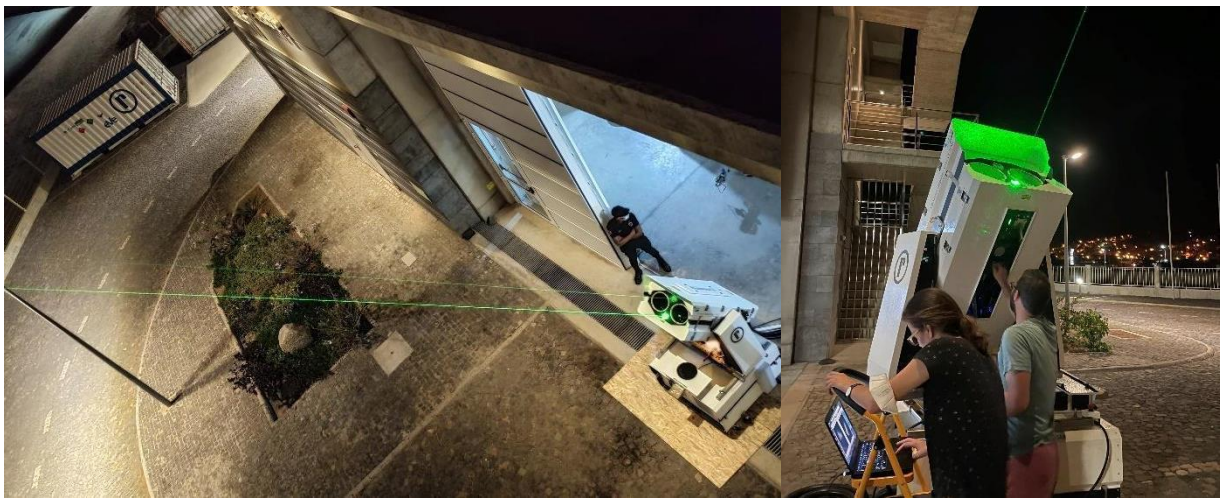

Figure 4.1: Operation of the eVe lidar during the ASKOS campaign.

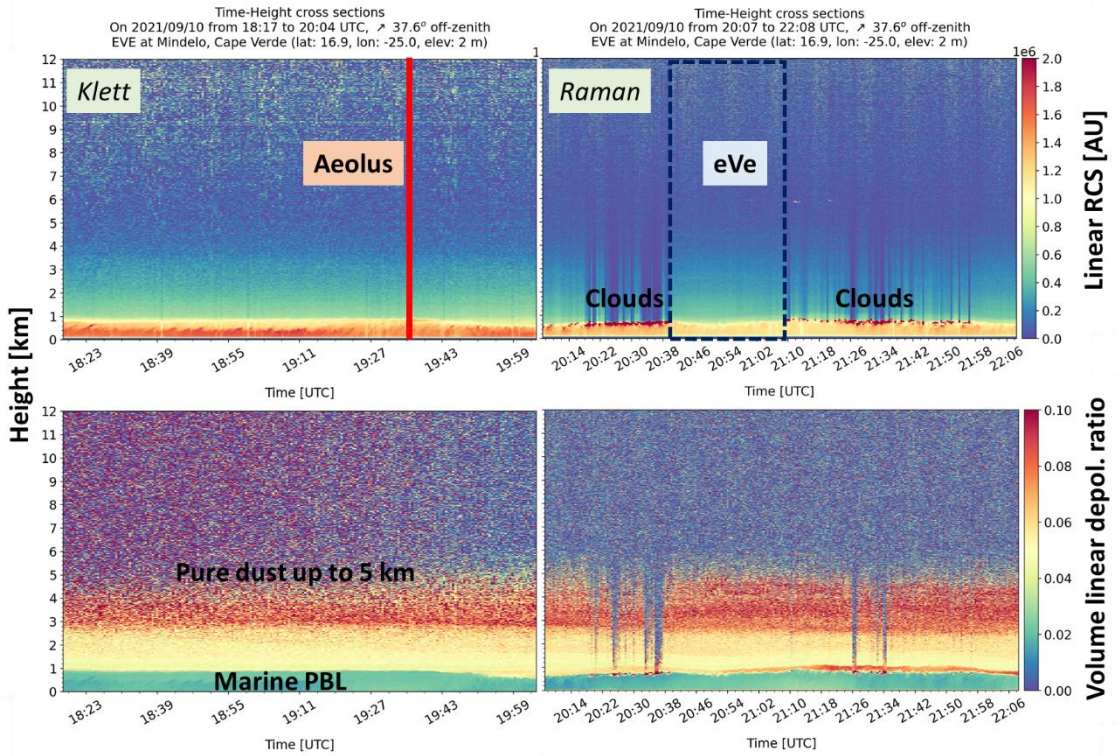

Figure 4.2: Time-height cross sections of the L1 products of the range-corrected signal and the volume linear depolarization ratio from eVe measurements on 10 September 2021.

The eVe is a combined linear/circular polarization lidar system with Raman capabilities that operates at 355 nm. The lidar is designed to be a mobile and flexible system and it is implemented in a dual-laser/dual-telescope configuration that can point at multiple azimuths and off-zenith angles allowing eVe to simultaneously reproduce the operation of the deployed lidar onboard Aeolus (ALADIN) which operates with circularly polarized emission at 355 nm as well as the operation of a traditional linear polarization lidar system. As such, the lidar can reproduce the operation and the pointing geometry of any lidar (spaceborne or ground-based) that emits linearly or circularly polarized light. The L1 eVe lidar products are the range-corrected lidar signals and the volume linear and circular depolarization ratios. The L2 eVe lidar products are the vertical profiles of the particle backscatter and extinction coefficients and lidar ratio retrieved using the linear and the circular emission, and the linear and circular depolarization ratios at 355 nm. Additionally, to the L2 products, eVe is able to directly retrieve the Aeolus-like backscatter coefficient and Aeolus-like lidar ratio which are the ground-based lidar products that will be used in the L2A+ validation. An example plot of the available eVe products is provided in Figure 4.3.

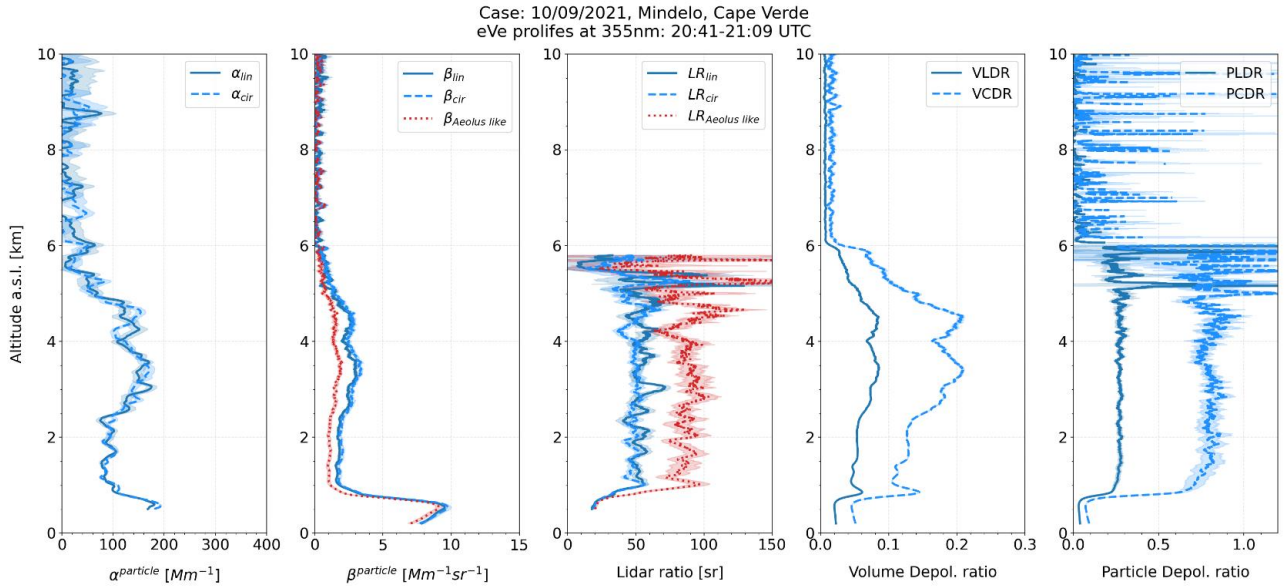

Figure 4.3: The L2 eVe products from the collocated measurement with Aeolus during the nearest Aeolus overpass on Friday 10 September 2021.

4.2. PollyXT lidar.

The PollyXT lidar is provided by TROPOS and it is an automated multiwavelength Raman polarization and water vapor lidar capable of measuring the aerosol loads in the boundary layer and the free troposphere. The lidar operates with 3 elastic backscatter channels (355, 532, 1064 nm), 3 Raman extinction channels (387, 607, 1058 nm), 3 depolarization channels (355, 532, 1064 nm) and one water–vapor sensitive channel (407 nm). The near-range receiver with 4 channels (elastic and Raman at 355 nm, elastic and Raman at 532 nm) provides a full overlap above 100 m allowing the detection of particles at low altitudes. The L1 measured parameters of the lidar are the range-corrected lidar signals at all operating wavelengths as well as the attenuated backscatter signals (Figure 10). The L2 PollyXT lidar products are the profiles of the particle backscatter and extinction coefficients at 355, 532, 1064 nm, the lidar ratio at 355 and 532 nm, the volume and particle linear depolarization ratios at 355 and 532 nm, the angstrom exponent (355/532 nm, 532/1064 nm), and the water vapor mixing ratio (Figure 4.4).

The PollyXT along with the rest instrumentation provided by TROPOS (microwave radiometer, wind lidar, sun-photometer) have been transported from Leipzig, Germany to Mindelo, Cabo Verde and have been installed at the OSCM from the TROPOS personnel. The lidar is housed inside the OSCM, thus it can be operated under various climatic conditions.

Figure 4.4: The PollyXT lidar during the ASKOS operations at the OSCM.

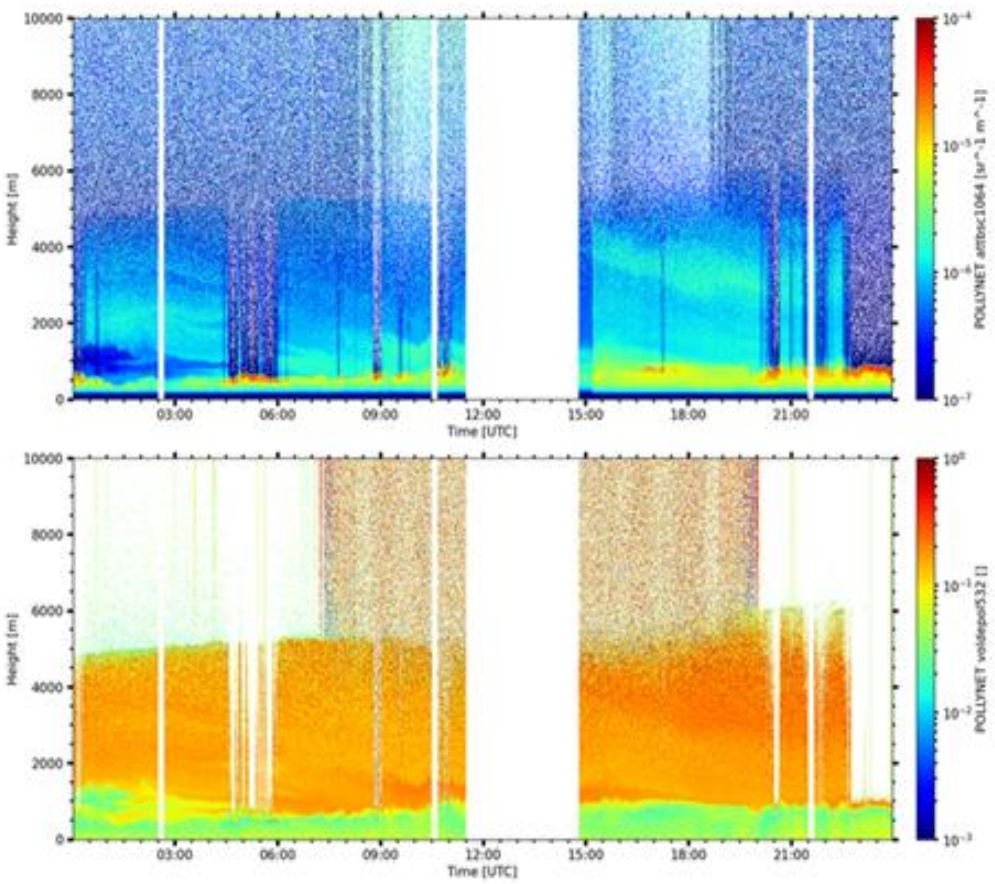

Figure 4.5: Range-corrected signal at 1064 nm (top) and linear volume depolarization ratio at 532 nm (bottom) above Mindelo on 10 September 2021.

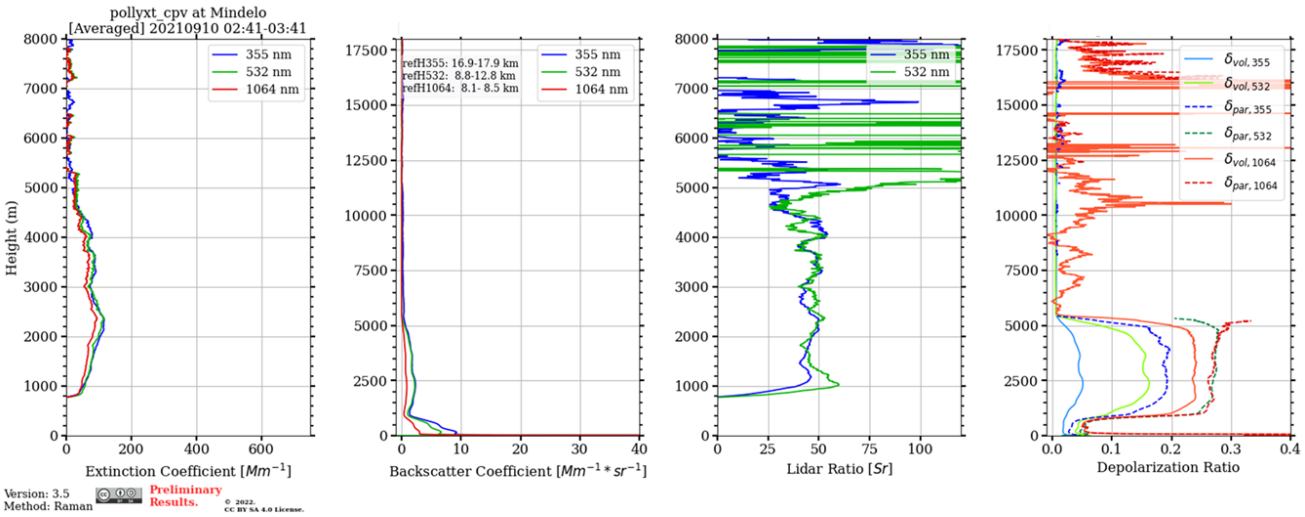

Figure 4.6: Vertical profiles of the particle extinction and backscatter coefficient, particle lidar ratio, volume depolarization and particle linear depolarization ratio measured at Mindelo on 10 September 2021, from 02:41-03:41 UTC.

5. ESA-L2A+ WP3000: Validation of the L2A+ aerosol product.

In this part, the results of the L2A+ WP3000 will be presented for three indicative Aeolus overpasses over Mindelo, Cabo Verde and specifically on the 10th, 17th, and 24th of September 2021 due to the availability of the corresponding ground-based retrievals acquired by the eVe and PollyXT lidars which were operated for validation purposes in the framework of the JATAC campaign. Our results include among others the following: the raw Aeolus L2A retrievals retrieved from multiple algorithms including the Standard Correct Algorithm (SCA), the SCA mid-bin and MLE algorithms, the cloud-filtered Aeolus L2A retrievals after eliminating all the cloud-contaminated profiles using both the AEL-FM feature mask product and the MSGG-SEVIRI CLASS-3 cloud dataset, the pure dust profiles identified using CAMS reanalysis outputs for dust-typing, the final Aeolus L2A+ product and the validation of the new Aeolus product against ground-based measurements acquired from eVe and PollyXT lidars. The results for each study case are summarized in the following sections.

5.1. The case of the 10th of September 2021.

5.1.1. Description of the atmospheric scene.

Figure 5.1a illustrates the L2A+ region of interest with the blue-colored line indicating the ascending ALADIN's measurement track for the given case. Next, Figure 5.1b illustrates for the specific study case, the time-closest binary cloud mask (CMa) product retrieved from the SEVIRI CLAAS-3 cloud dataset which as we can see in the figure, describes the scene type (either 'clear' or 'cloudy') on a pixel level. The Aeolus's ascending orbit is also depicted on the same figure with the red-colored line. Based on the specific cloud-filtering procedure, the Aeolus SCA, SCA mid-bin and MLE backscatter retrievals, throughout the probed atmosphere by ALADIN, have been excluded from the analysis when the cloud fraction in each BRC profile exceeds a given threshold value (60% in this case).

Aeolis Orbit

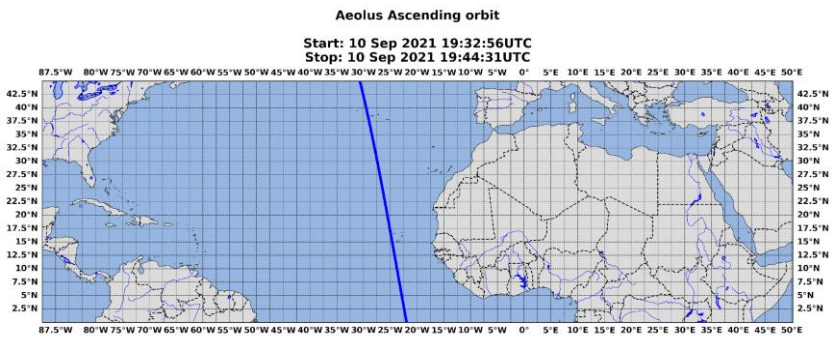

MSG Cloud Coverage

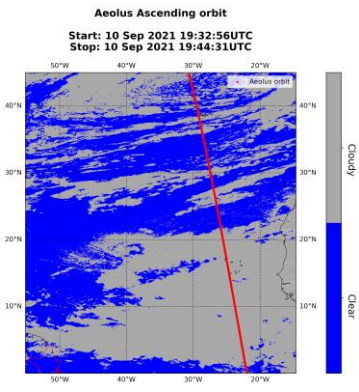

Figure 5.1: a) Aeolus ascending orbit (id: 017679) over the L2A+ RoI on 10th September 2021 and b) the time-closest spatial distribution of clouds derived from the binary cloud-mask product of MSG-SEVIRI CLAAS-3 dataset.

In Figure 5.2a, the retrieved AEL-FM feature-mask product along the given Aeolus's measurement track is presented where we can observe the classified features of the probed atmospheric scene. It can be seen that the features associated with "strong" returns mainly attributed to clouds or high optically thick aerosol layers are colorized in brown and orange respectively while those associated

with the molecular atmosphere or clear sky conditions are colorized in green and cyan respectively. According to the figure, one can clearly distinguish a large number of strong features that have been classified as (likely and most likely) clouds (FM values of 6 to 10) along the largest part of the given Aeolus's measurement track and especially between latitudes of 0 and 7◦ N and altitudes between 4 and 14 km above the ground. Following our filtering methodology, these features can be detected and excluded from the analysis in order to acquire the pure aerosol profiles. In the two figures below, the transformed feature mask product to the Aeolus's horizontal and vertical resolution is provided separately for the regular Aeolus's vertical scale (24 vertical bins) (Figure 5.2b) and middle-bin (23 vertical bins) scale (Figure 5.2c) with each bin expressing the cloud fraction (in %) of the specific BRC bin after computing the total percentage of cloud-contaminated measurements for the specific bin. Based on the transformed feature mask product, all Aeolus's BRC bins with cloud fraction exceeding 0% were excluded from the analysis with the corresponding bins of the SCA, SCA mid-bin and MLE backscatter profiles.

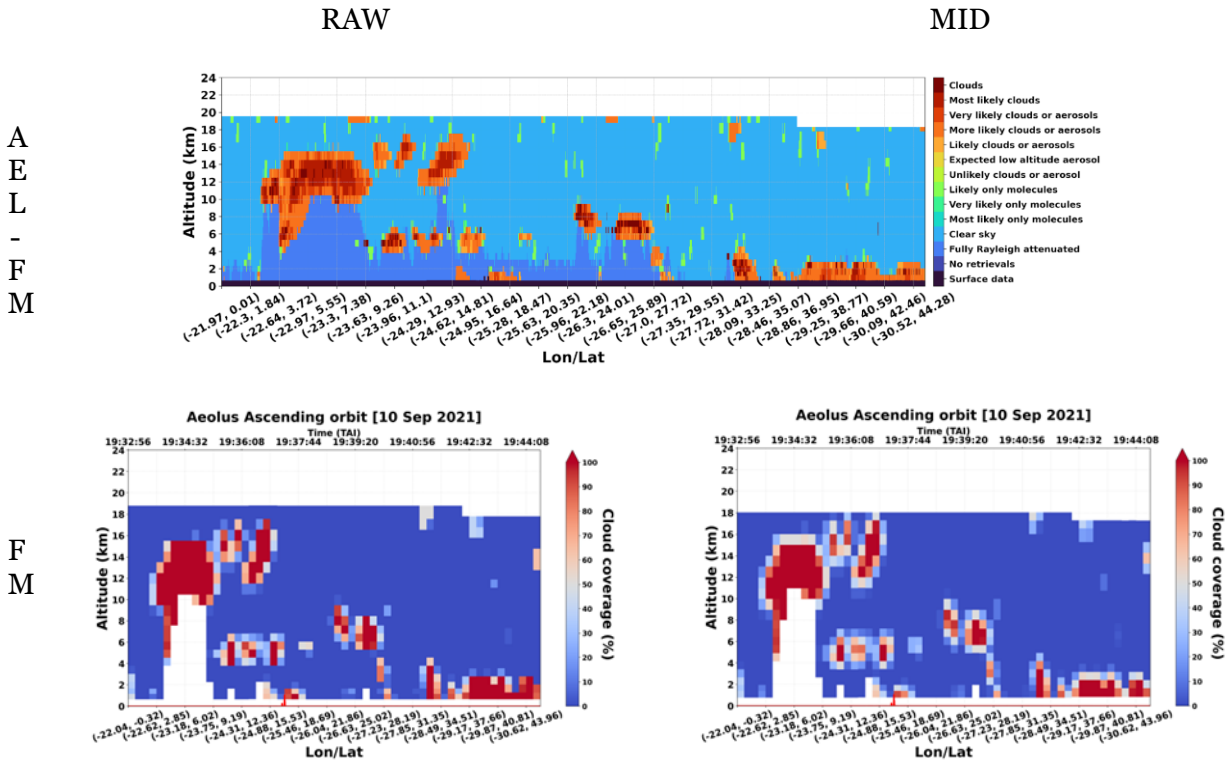

Figure 5.2: a) AEL-FM feature mask product along the Aeolus orbit (id: 017679) on 10th September 2021 and the transformed feature mask product on the Aeolus vertical and horizontal resolution for the b) regular (24 bins) and c) middle-bin scale (23 bins).

In the figure below, we present the horizontally integrated and vertically resolved Aeolus-like dust mass concentration profiles from CAMS along the Aeolus orbit (id: 017679), provided separately for the regular (Figure 5.3a) and middle-bin (Figure 5.3c) Aeolus' vertical scales (24, and 23 vertical bins respectively). According to the figure, a dust layer is identified over the latitudinal band of 5°- 25°N and up to 6km with elevated dust mass concentration values exceeding in many cases the value of 50 μg/m^3. Additionally, for both vertical scales, the vertical profiles of the dust-to-total mass concentration ratio values (in percentage) along the Aeolus measurement track are also depicted in Figures 5.3b, and d. Based on both parameters retrieved from CAMS, the pure dust profiles were derived after eliminating all the BRC bins with dust concentration below 1.3 μg/m^3 (median value) and dust-to-total ratio below 50%.

Dust Mass Concentration (µg/m3)

Dust Percentage (%)

RAW

MID

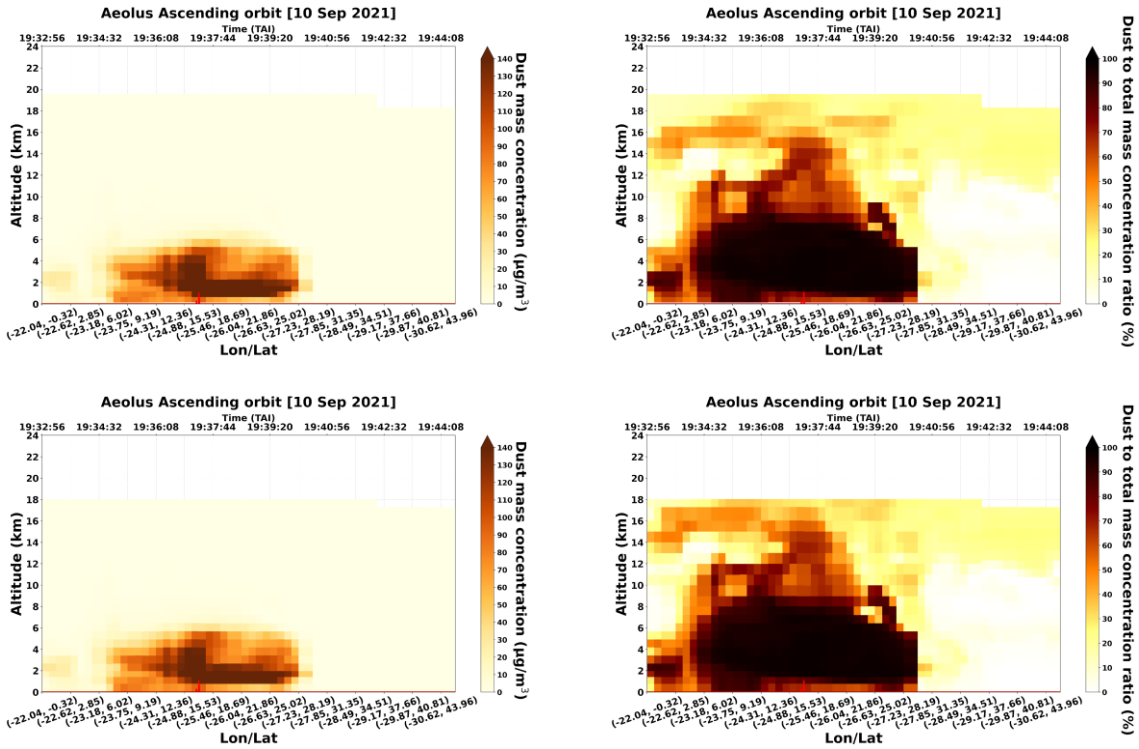

Figure 5.3: Vertical profiles of CAMS dust mass concentration and dust-to-total aerosol mass concentration ratio along the Aeolus orbit (id: 017679) provided in the regular (a, b) and middle-bin (c, d) vertical scales on the 10th of September 2021.

For the specific study case, the time-closest vertical profiles of CALIPSO total backscatter coefficient at 532 nm (Figure 5.4a), particulate depolarization ratio at 532 nm (Figure 5.4b) and the quality-assured (QA) pure-aerosol (Figure 5.4c) and pure-dust backscatter coefficient (Figure 5.4d) are also illustrated.

CALIPSO Total b532 nm ($km^{-1}sr^{-1}$)

CALIPSO d532nm

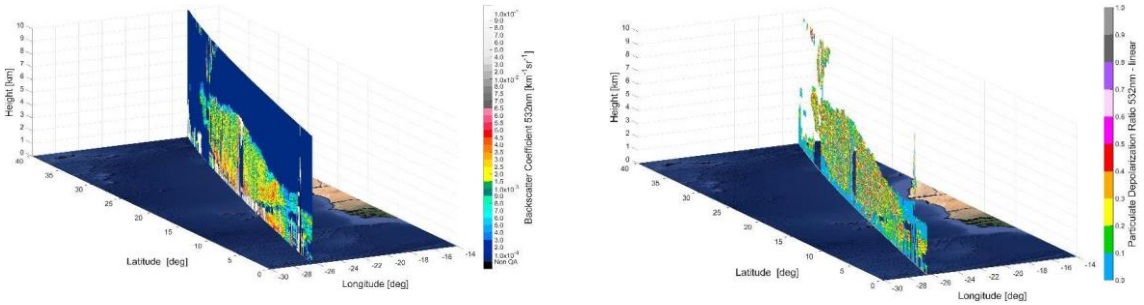

CALIPSO Total b532 nm – QA (km^{-1}sr^{-1})

LIVAS Pure-Dust b532nm – QA (km^{-1}sr^{-1})

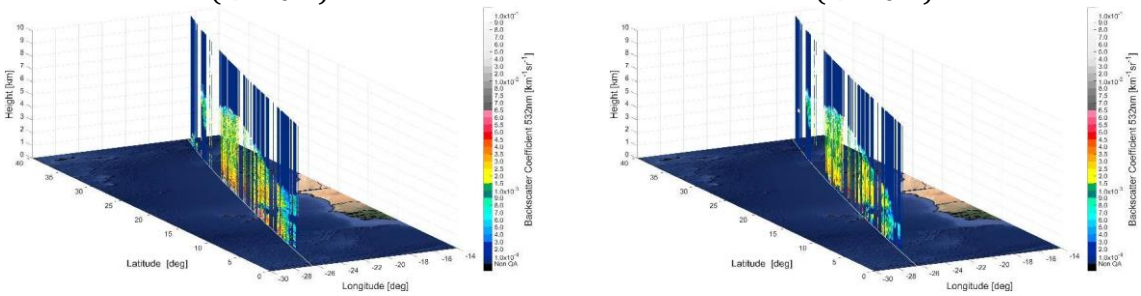

Figure 5.4 (a) CALIPSO total backscatter coefficient at 532 nm. (b) CALIPSO particulate depolarization ratio at 532 nm (c) CALIPSO QA pure-aerosol total backscatter coefficient at 532 nm (d) CALIPSO QA pure-dust backscatter coefficient at 532 nm.

5.1.2. Aeolus Optical Products.

In figure 5.5, the left panel illustrates the vertical profiles of the raw (unprocessed) Aeolus L2A retrievals of backscatter coefficient at 355 nm along the Aeolus overpass (id 017679), produced by the SCA, SCA mid-bin and MLE algorithms, while the right panel depicts the quality-assured (QA) backscatter profiles derived from the corresponding algorithms after implementing the cloud-filtering methodology using both the AEL-FM feature mask and MSG-SEVIRI Claas-3 cloud-mask retrievals. It has to be noted that the later ones correspond to the pure-aerosol backscatter profiles along the Aeolus overpass, since most of bins were rejected from the cloud-filtering process.

Aeolus b355nm - Raw (Mm^{-1}sr^{-1})

Aeolus b355nm – AEL-FM & MSG QA (Mm^{-1}sr^{-1})

SCA

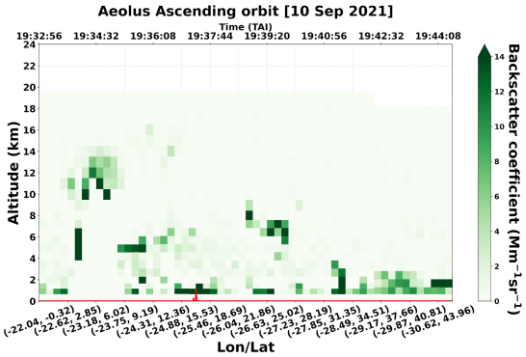

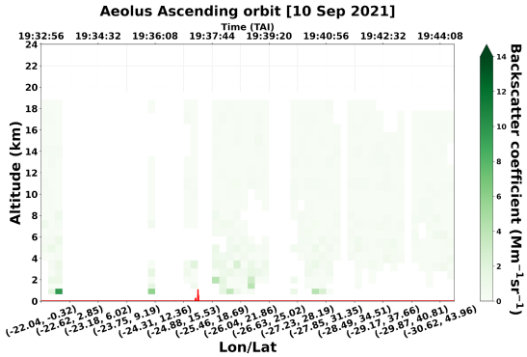

SCAMID-BIN

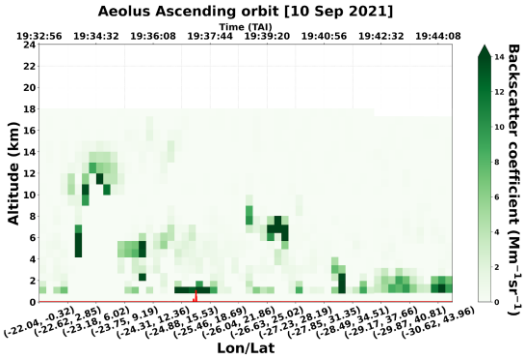

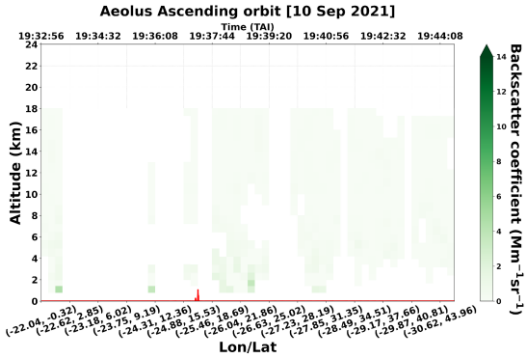

MLE

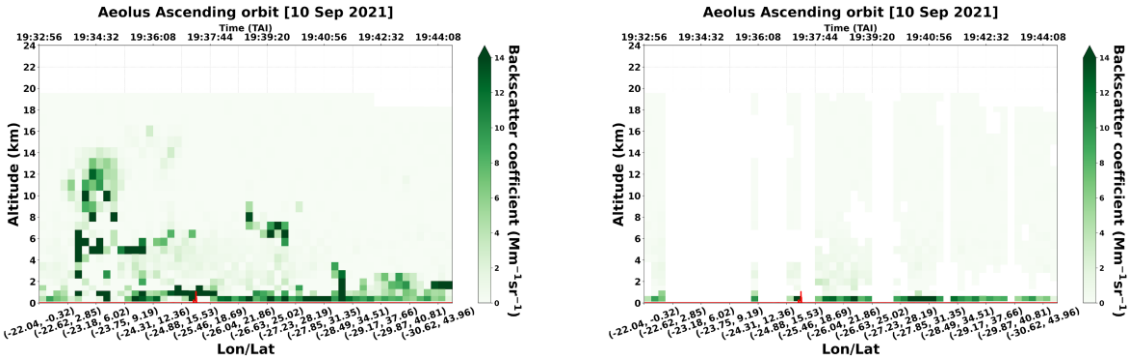

Figure 5.5 Raw Aeolus L2A backscatter profiles at 355 nm along the Aeolus orbit (id 017679) retrieved from the SCA, SCA mid-bin and MLE algorithms (left panel) and the corresponding QA pure-aerosol backscatter profiles at 355 nm for the SCA, SCA mid-bin and MLE algorithms (right panel).

5.1.3. L2A and L2A+ products.

Figure 5.6 gives for the given study case, an example of the pure-dust Aeolus co-polar backscatter profiles at 355 nm produced with the SCA and SCA mid-bin algorithms and the associated missing cross-polar backscatter component for each profile. Using both backscatter components (co + cross) the total (L2A+) backscatter profiles at 355 nm were derived and were used for the reconstruction of the pure-dust L2A extinction coefficient.

Aeolus b355nm – co ($Mm^{-1}Sr^{-1}$)

Aeolus b355nm – cross ($Mm^{-1}Sr^{-1}$)

SCA

SCA mid-bin

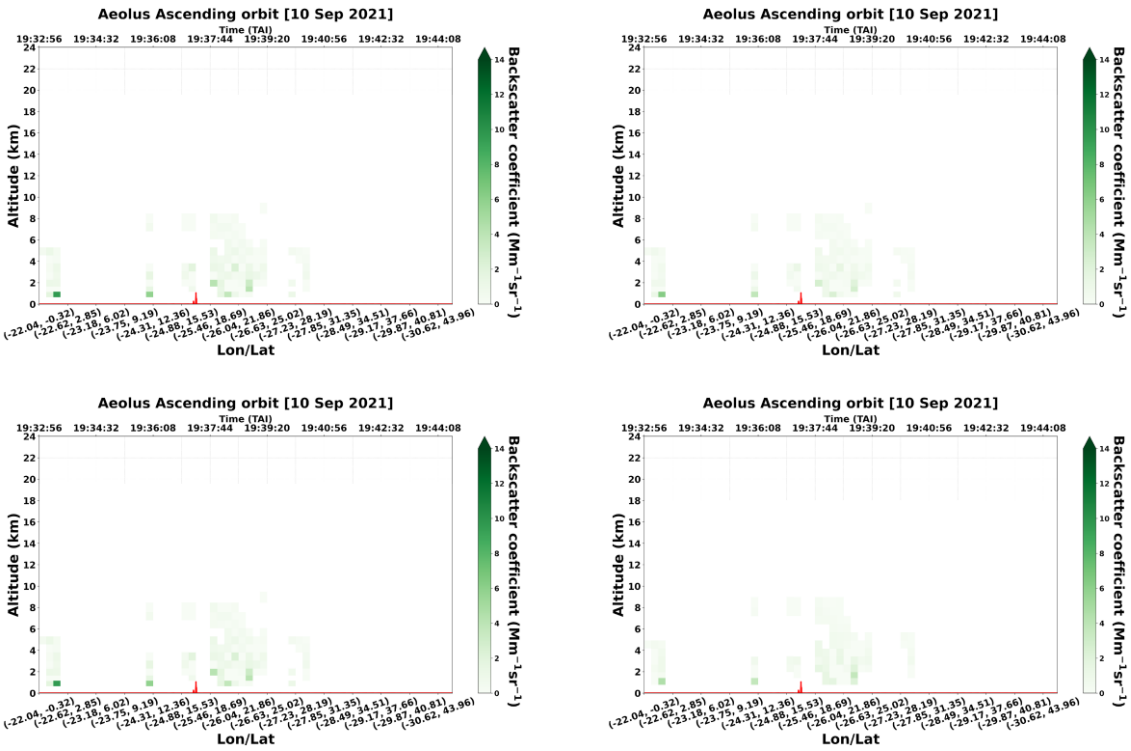

Figure 5.6: Co-polar and cross polar backscatter profiles along the Aeolus overpass (id 017679) for the SCA (a, b) and SCA mid-bin algorithms (c, d).

5.1.4. L2A+ - ESA-eVe validation.

The present section gives the intercomparison of Aeolus L2A and L2A+ aerosol optical products, in particular the backscatter coefficient at 355 nm retrieved with the SCA, SCA mid-bin and MLE algorithms against ground-based measurements from eVe lidar collected during the ASKOS experiment, under the Joint Aeolus Tropical Atlantic Campaign 2021 (JATAC), on the islands of Cabo Verde. The process was performed considering the raw (unprocessed) Aeolus L2A co-polar backscatter profiles at 355 nm for each of the aforementioned algorithms (SCA, SCA mid-bin, MLE) and the quality-assured (QA) pure-dust total (L2A+) backscatter profiles at 355 nm after the adjustment of the missing cross-polar component. It has to be noted that only the quality-assured (cloud-free) ground-based measurements were used for the comparison process. Moreover, only three study cases will be presented for the intercomparison process which serve as graphic examples of the Aeolus performance and here we start with the first study case on 10th September 2021 presented in Figure 5.7.

According to our results, comparing the raw (left panel) and the QA Aeolus retrievals (right panel), it can be noticed that the implementation of the cloud-filtering and dust-typing methodologies for the derivation of the new Aeolus product (L2A+) produces a notable decrease in the amount of available data points since most of bins were rejected from the analysis. This can be noticed at around 6km where the large backscatter coefficients of the raw Aeolus L2A retrievals mostly attributed to cloud presence have been excluded in the QA retrievals. Moreover, looking at the raw Aeolus L2A retrievals, it can also be noticed a surface-related effect in the lowermost bins, retrieving an unreasonably large co-polar backscatter coefficient which was also rejected in the QA retrievals.

Next, focusing on the pure-dust layers of Aeolus L2A and L2A+ retrievals in Figure 5.7 (right panel), it can be noticed that after the correction of the backscattered signal, the L2A+ backscatter profiles present a better agreement with ground-based measurements than L2A retrievals. Especially, a fair agreement between the Aeolus L2A+ backscatter profile for the MLE algorithm and the corresponding ground-based system is pointed out throughout the vertical range of the detected dust layer.

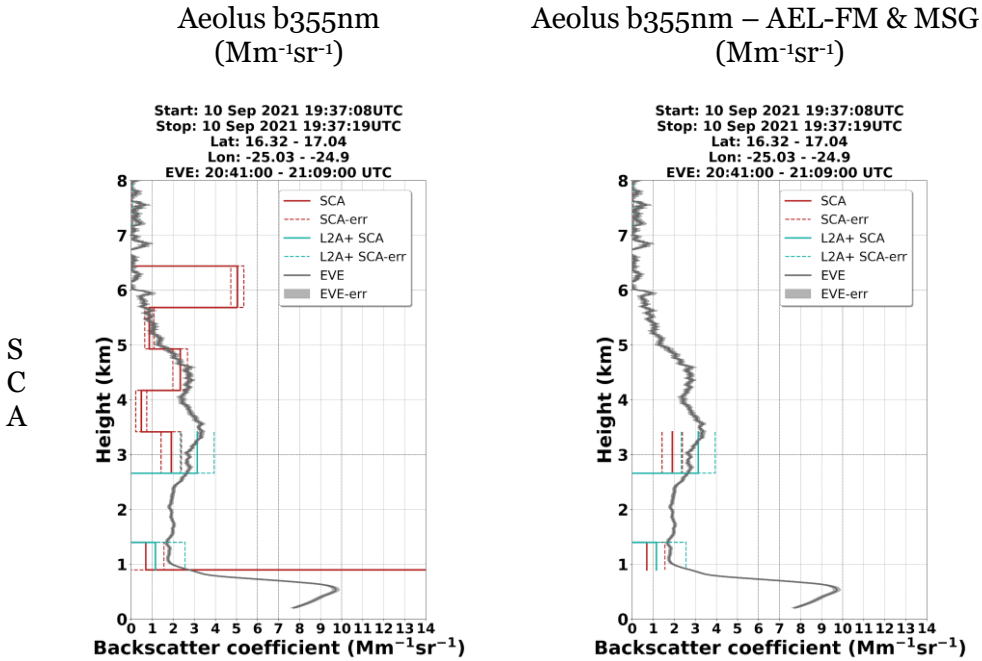

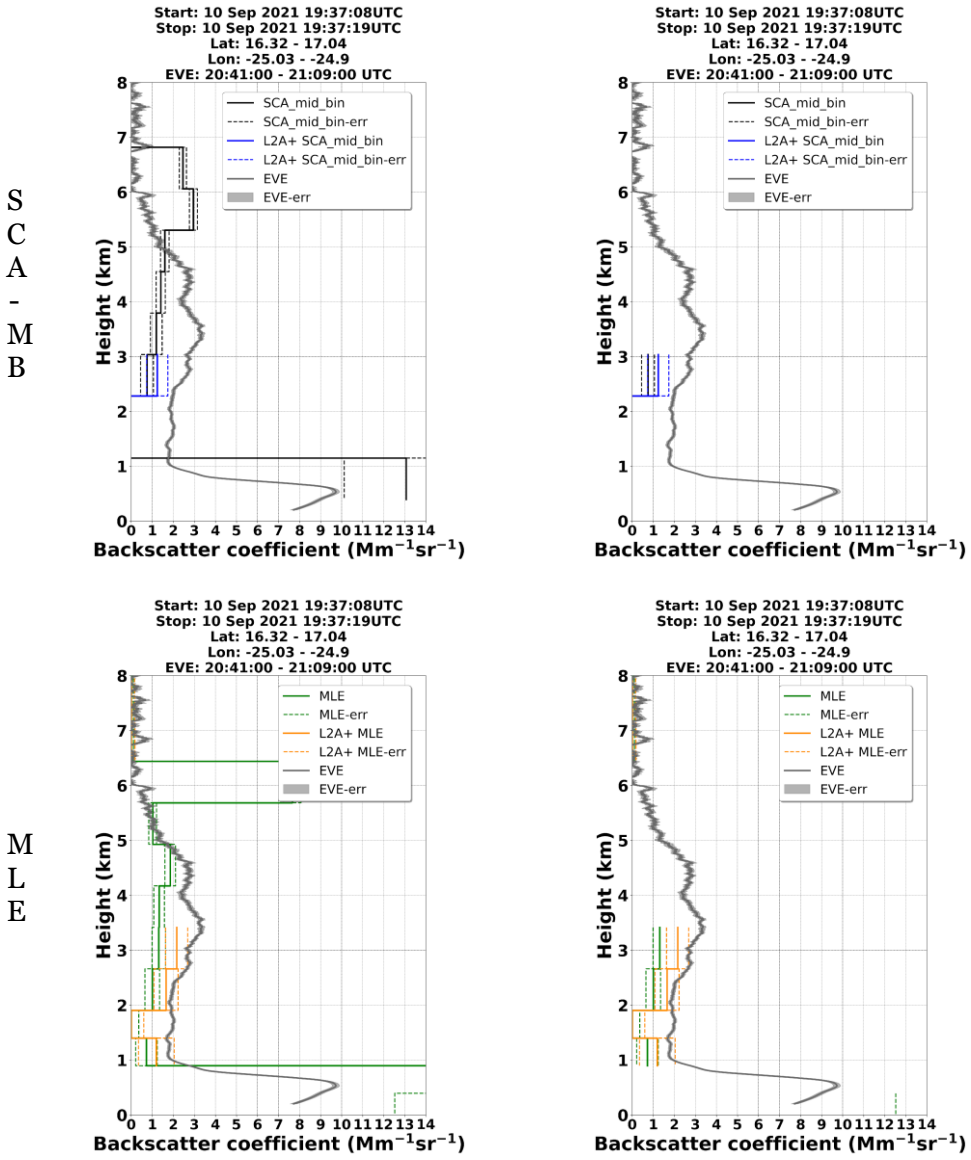

Figure 5.7: Vertical profiles of the raw Aeolus L2A and QA L2A+ backscatter coefficient at 355 nm retrieved from the SCA, SCA mid-bin and MLE algorithms with the corresponding backscatter profiles at 355 nm acquired by eVe ground-based lidar (left panel), and QA Aeolus L2A and L2A+ backscatter profiles for the SCA, SCA mid-bin and MLE algorithms with the derived backscatter profiles from eVe lidar (right panel).

5.1.5. L2A+ - ESA-PollyXT validation.

The same intercomparison process was also performed between the vertically resolved Aeolus L2A/L2A+ backscatter coefficient at 355 nm for the SCA, SCA mid-bin and MLE algorithms and the corresponding time-nearest backscatter profiles at 532 nm from the Polly^{XT} ground-based lidar operated at Mindelo station, Cabo Verde. The obtained results are presented in Figure 5.8 for the given study case on 10th September 2021. According to the results, we point out for the pure-dust layers (right panel), that for all the Aeolus L2A retrieval algorithms including the SCA, SCA mid-bin and MLE algorithms, the backscatter coefficient is underestimated throughout the whole vertical

range of the detected dust layer. This difference is mostly attributed to the misdetection of the cross-polar component of the backscattered lidar signal when non-spherical mineral particles are recorded. Gkikas et al. (2023) also presented an underestimation that reached up to 33% in the aerosol backscatter coefficient after comparing the PollyXT and Aeolus-like PollyXT backscatter profiles for a study case on 10th July 2019 corroborating our findings. On the other hand, based on our results we can see that this difference is minimized and the satellite presents a satisfactory agreement with PollyXT lidar in the whole available profile when comparing the corrected L2A+ pure-dust total backscatter coefficient with the PollyXT-derived backscatter profile for all the available algorithms.

	Aeolus b355nm ($Mm^{-1}sr^{-1}$)	Aeolus b355nm – AEL-FM & MSG QA ($Mm^{-1}sr^{-1}$)
SCA	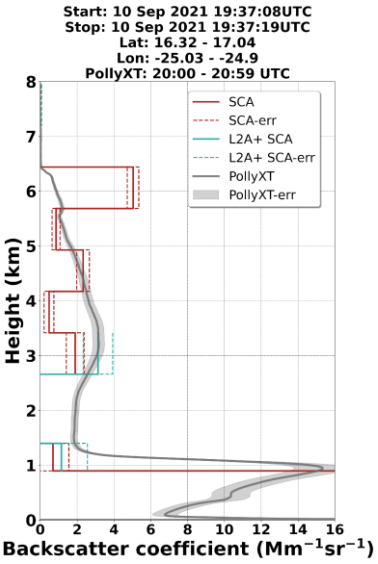	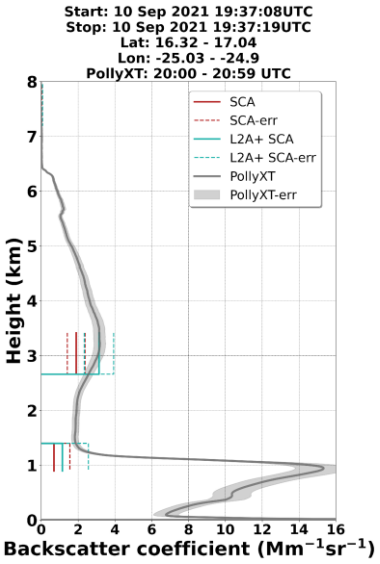
SCA-MB	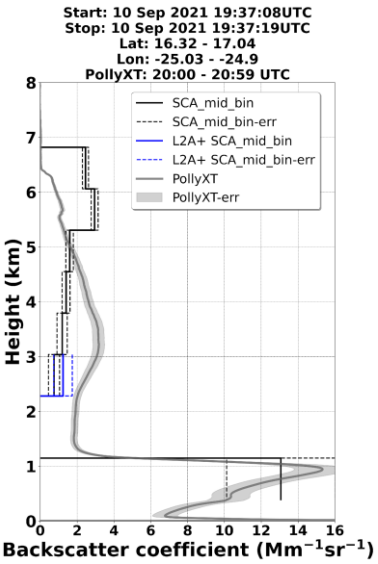	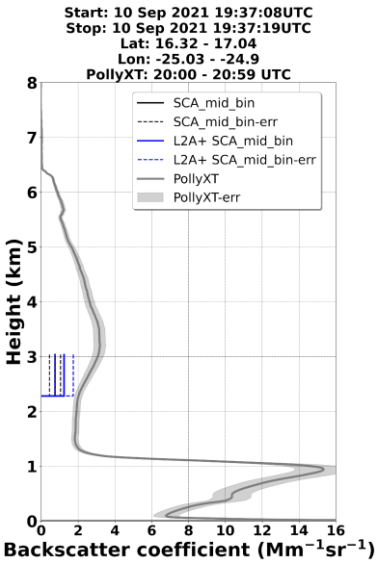

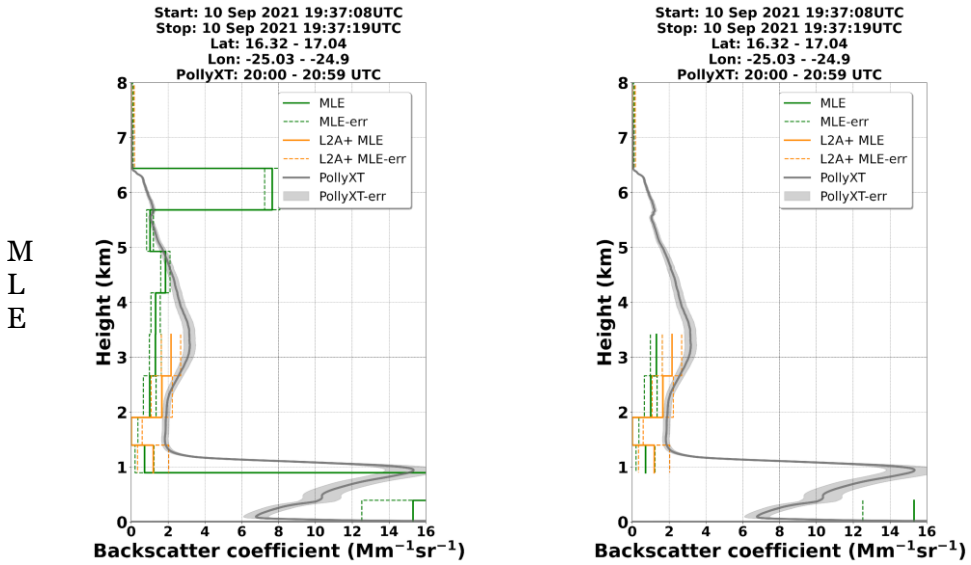

Figure 5.8: Vertical profiles of the raw Aeolus L2A and QA L2A+ backscatter coefficient at 355 nm retrieved from the SCA, SCA mid-bin and MLE algorithms with the corresponding backscatter profiles at 355 nm acquired by PollyXT ground-based lidar (left panel), and QA Aeolus L2A and L2A+ backscatter profiles for the SCA, SCA mid-bin and MLE algorithms with the derived backscatter profiles from PollyXT lidar (right panel).

5.2. The case of the 17th of September 2021.

5.2.1. Description of the atmospheric scene.

In the current section, we present our results for the second study case on 17th September 2021. Figure 5.9 illustrates the ascending ALADIN's measurement track on the given case (id 017790), the time-nearest spatial distribution of the "clear" and 'cloudy' areas on a pixel level acquired from the MSG-SEVIRI CLAAS-3 cloud dataset, the AEL-FM feature mask product retrieved for the specific atmospheric scene and the transformed AEL-FM product to the Aeolus BRC scale (~90 km horizontal resolution each BRC profile) giving the cloud-fraction (in %) of each BRC profile.

Aeolis Orbit MSG Cloud Coverage

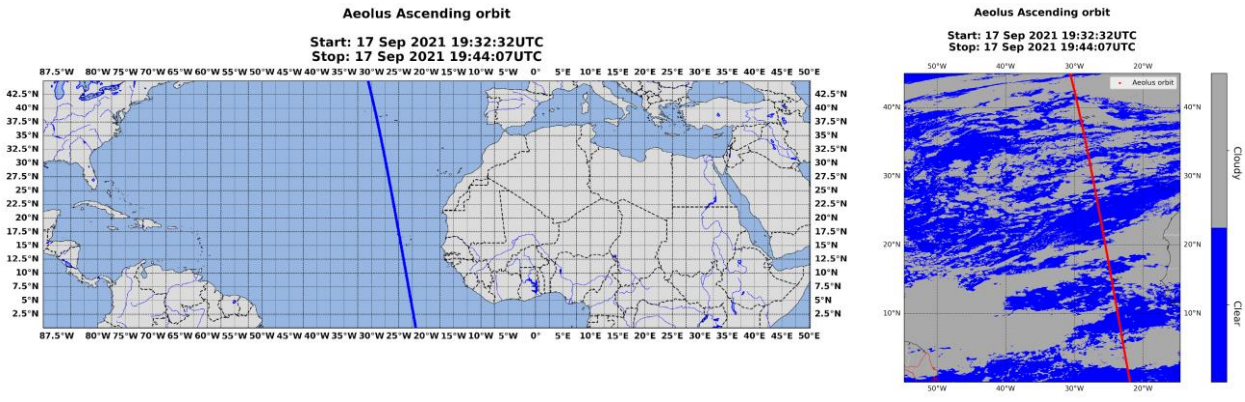

AEL-FM

FM

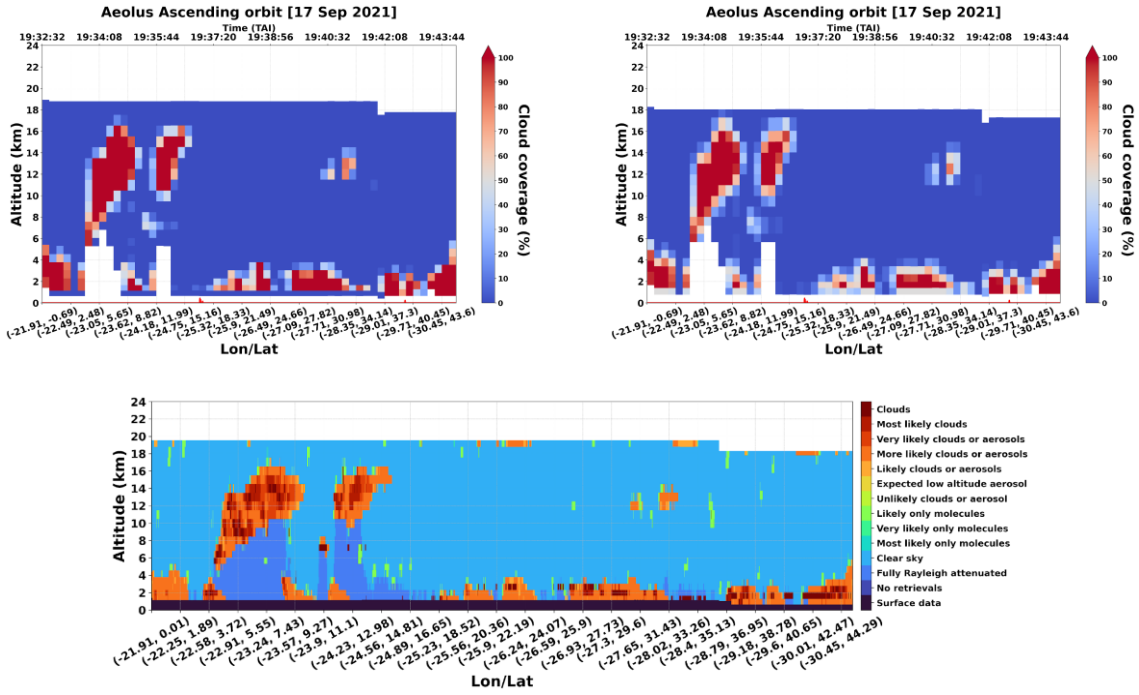

Figure 5.9: Aeolus ascending orbit (id: 017790) over the L2A+ RoI on 17th September 2021 and the time-closest spatial distribution of "cloudy" and "clear" pixels derived from the binary cloud-mask product of MSG-SEVIRI CLAAS-3 dataset (upper panel). The transformed AEL-FM product to the Aeolus BRC scale for the regular (24 bins) and middle-bin vertical scale (23 bins) (middle panel) and the AEL-FM feature mask product at the Aeolus measurement scale (~3km horizontal resolution) with the classified features of the probed atmospheric scene.

In the figure below, we present for both vertical scales (regular and middle-bin scale), the vertically resolved profiles of dust mass concentration acquired from CAMS along the referenced Aeolus orbit (id: 017790). Additionally, for both vertical scales, the vertical profiles of the dust-to-total mass concentration ratio values (in percentage) along the Aeolus measurement track are also depicted in Figures 5.10b, and d. Based on the figure, a dust layer is identified over the latitudinal band of 5°-15°N and up to 6km with elevated dust mass concentration and dust-to-total concentration ratio values.

RAW

Dust Mass Concentration (μg/m3)

Dust Percentage (%)

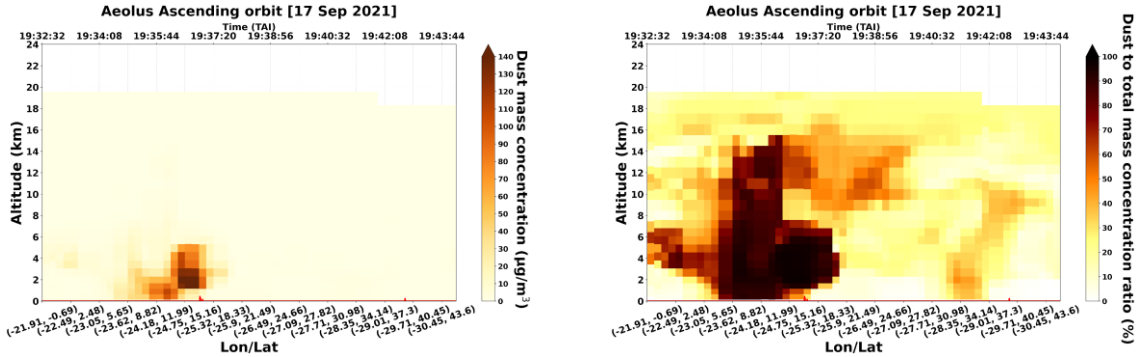

M
I
D

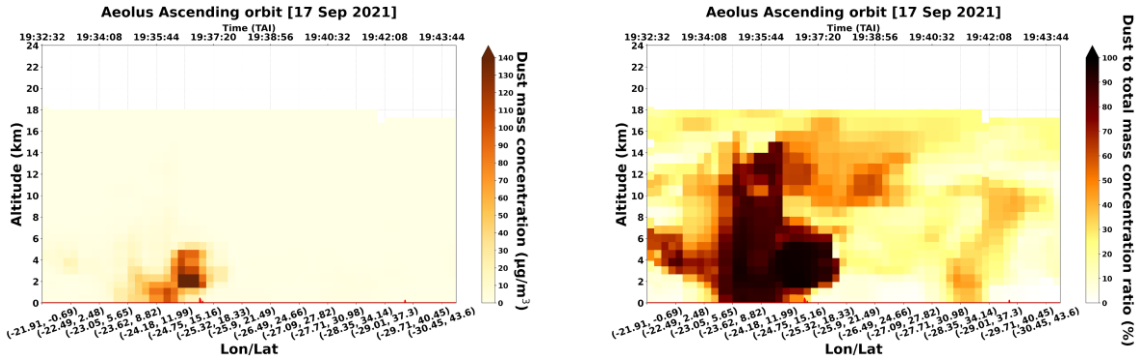

Figure 5.10: Vertical profiles of CAMS dust mass concentration and dust-to-total aerosol mass concentration ratio along the Aeolus orbit (id: 017790) provided at the regular (a, b) and middle-bin (c, d) vertical scales for the study case on the 17th of September 2021.

Moreover, the time-nearest vertical profiles of CALIPSO total backscatter coefficient at 532 nm (Figure 5.11a), particulate depolarization ratio at 532 nm (Figure 5.11b) and the quality-assured (QA) pure-aerosol (Figure 5.11c) and pure-dust backscatter coefficient (Figure 5.11d) are also illustrated in the figure below.

CALIPSO Total b532 nm ($km^{-1}sr^{-1}$)

CALIPSO d532nm

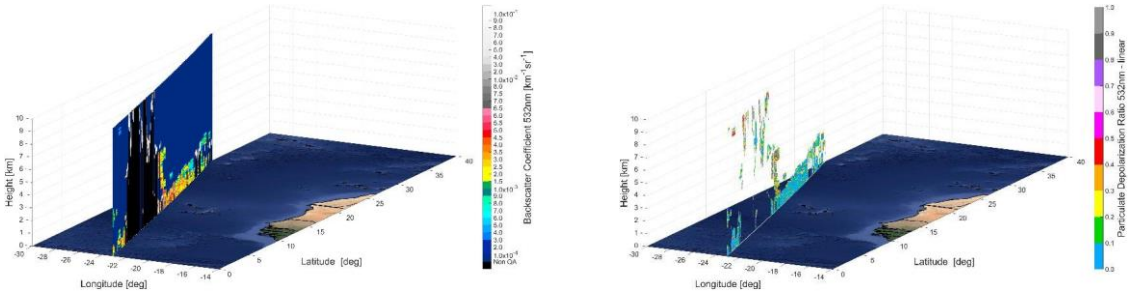

CALIPSO Total b532 nm – QA ($km^{-1}sr^{-1}$)

LIVAS Pure-Dust b532nm – QA ($km^{-1}sr^{-1}$)

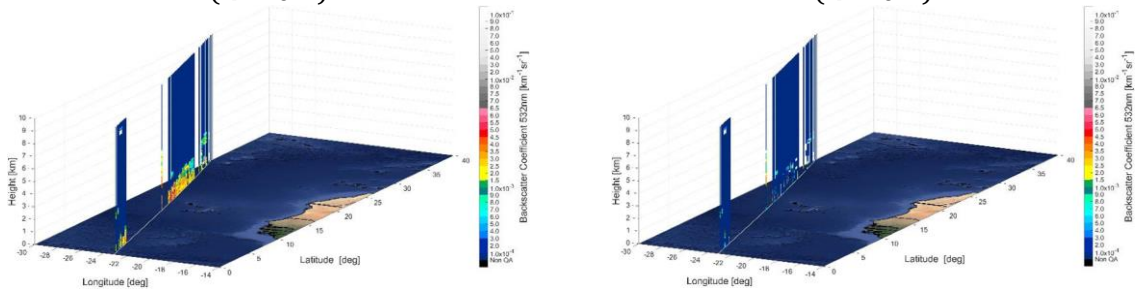

Figure 5.11 (a) CALIPSO total backscatter coefficient at 532 nm. (b) CALIPSO particulate depolarization ratio at 532 nm (c) CALIPSO QA pure-aerosol total backscatter coefficient at 532 nm (d) CALIPSO QA pure-dust backscatter coefficient at 532 nm. Study case: 17th September 2021.

5.2.2. Aeolus Optical Products.

Similarly, in Figure 5.12, the vertical profiles of the raw (left panel) and QA (right panel) pure-aerosol Aeolus L2A retrievals of backscatter coefficient at 355 nm along the Aeolus overpass (id 017790) are presented, separately for each of the three retrieval algorithms (SCA, SCA mid-bin and MLE), after implementing the cloud-filtering methodology using both the AEL-FM feature mask and MSG-SEVIRI Claas-3 cloud-mask retrievals.

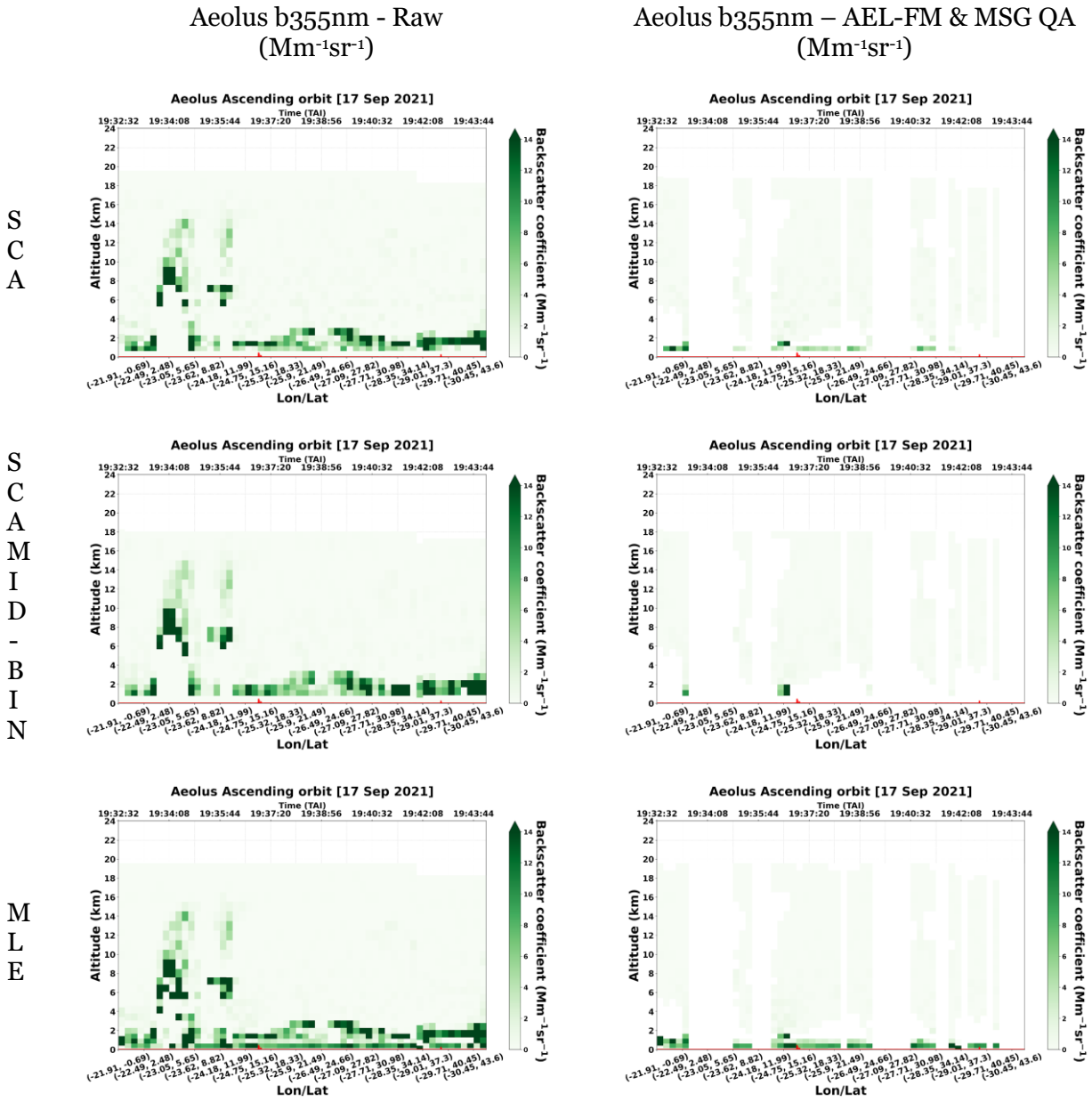

Figure 5.12 Raw Aeolus L2A backscatter profiles at 355 nm along the Aeolus orbit (id 017790) retrieved from the SCA, SCA mid-bin and MLE algorithms (left panel) and the corresponding QA pure-aerosol backscatter profiles at 355 nm for the SCA, SCA mid-bin and MLE algorithms (right panel).

5.2.3. L2A and L2A+ products.

Figure 5.13 illustrates for the given study case the pure-dust Aeolus co-polar backscatter profiles at 355 nm produced with the SCA and SCA mid-bin algorithms and the associated missing cross-polar backscatter component for each profile.

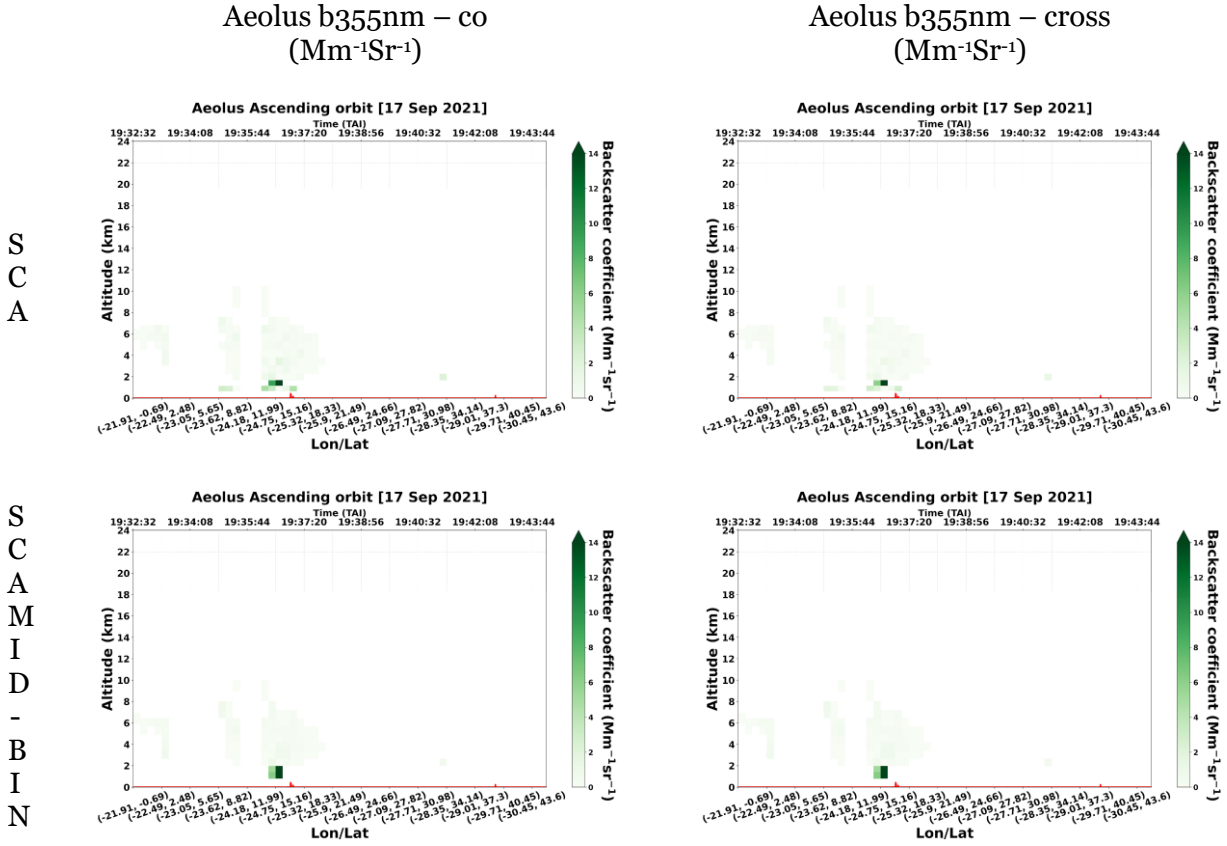

Figure 5.13: Co-polar and cross polar backscatter profiles along the Aeolus overpass (id 017790) for the SCA (a, b) and SCA mid-bin algorithms (c, d).

5.2.4. L2A+ - ESA-eVe validation.

The present section assesses for the second study case on 17th September 2021, the performance of the Aeolus L2A and L2A+ retrievals by comparing the SCA, SCA mid-bin and MLE backscatter profiles at 355 nm with ground-based measurements acquired from eVe lidar. The results are illustrated in Figure 5.14. At first glance, it is evident the difference between the raw (left panel) and QA (right panel) Aeolus L2A backscatter profiles which is attributed to the reduced number of vertical bins in the latter case after the rejection of the cloud-contaminated bins. Focusing on the lowermost dust layer found in the altitudes between 0 and 1 km, the Aeolus L2A+ total backscatter coefficient retrieved by the SCA algorithm seems to be largely overestimated by about 2 $Mm^{-1}sr^{-1}$ when compared with the ground-based retrieved backscatter coefficient from eVe lidar. Regarding the Aeolus L2A retrievals, it can be noticed that the co-polar backscatter coefficient derived from SCA algorithm is slightly underestimated compared with the eVe lidar. On the contrary, using the MLE algorithm, the L2A+ total backscatter coefficient presents quite a satisfactory agreement with the eVe lidar minimizing the difference between the co-polar L2A backscatter coefficient and the ground-based backscatter coefficient on the specific bin. Regarding the SCA retrieval algorithm at

the middle bin scale (middle panel), the lowermost bin has been rejected from the filtering process, thus, no conclusions can be derived from the intercomparison process.

	Aeolus b355nm ($Mm^{-1}sr^{-1}$)	Aeolus b355nm – AEL-FM & MSG QA ($Mm^{-1}sr^{-1}$)
SCA	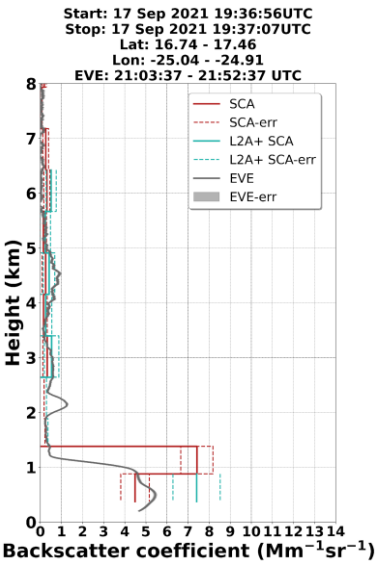	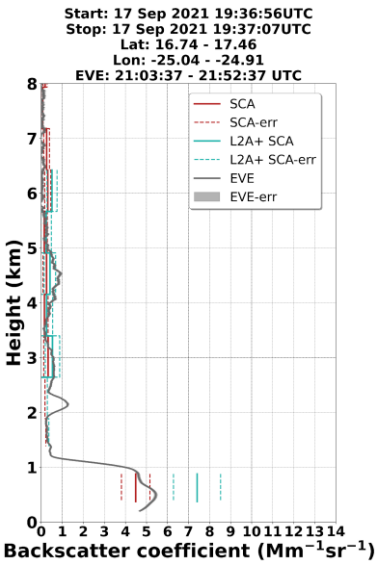
SCA-MB	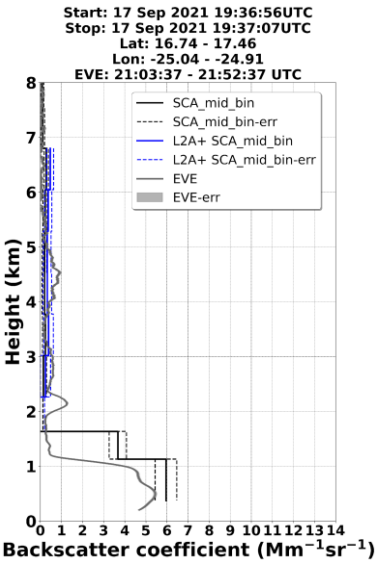	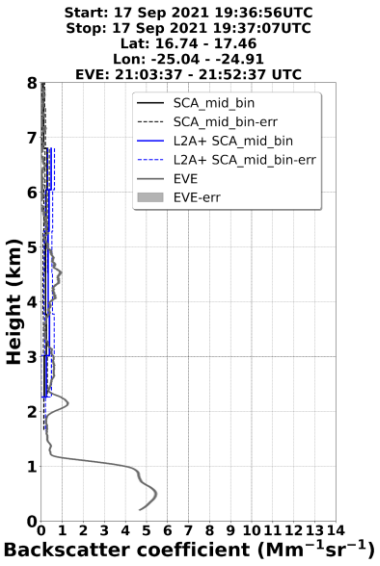

MLE

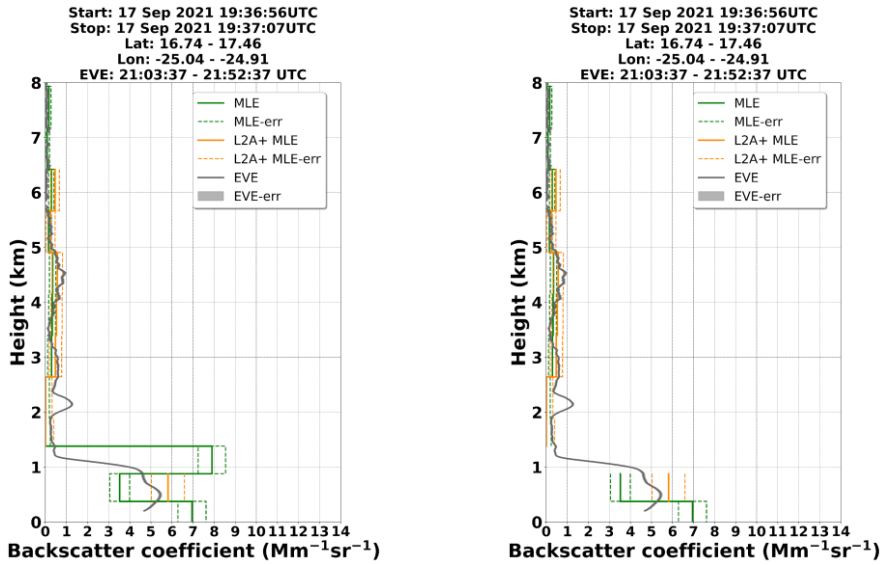

Figure 5.14: Vertical profiles of the raw Aeolus L2A and QA L2A+ backscatter coefficient at 355 nm retrieved from the SCA, SCA mid-bin and MLE algorithms with the corresponding backscatter profiles at 355 nm acquired by eVe ground-based lidar (left panel), and QA Aeolus L2A and L2A+ backscatter profiles for the SCA, SCA mid-bin and MLE algorithms with the derived backscatter profiles from eVe lidar (right panel).

5.2.5. L2A+ - ESA-PollyXT validation.

The intercomparison process was also performed between the Aeolus L2A/L2A+ vertical profiles of backscatter coefficient at 355 nm for the SCA, SCA mid-bin and MLE algorithms and the corresponding backscatter profiles at 532 nm from the Polly^{XT} ground-based lidar. The obtained results which are presented in Figure 5.15 for the study case on 10th September 2021, show that Aeolus presents quite a good agreement with the ground-based PollyXT lidar in the available pure-dust profiles when comparing the corrected SCA and MLE L2A+ total backscatter coefficient at 355 nm with the derived backscatter profile from PollyXT lidar at 532 nm. However, it has to be noted that no safe conclusions can be drawn from the intercomparison process of the specific case study since the implemented filtering tools in the raw Aeolus L2A retrievals have significantly reduced the number of available Aeolus bins.

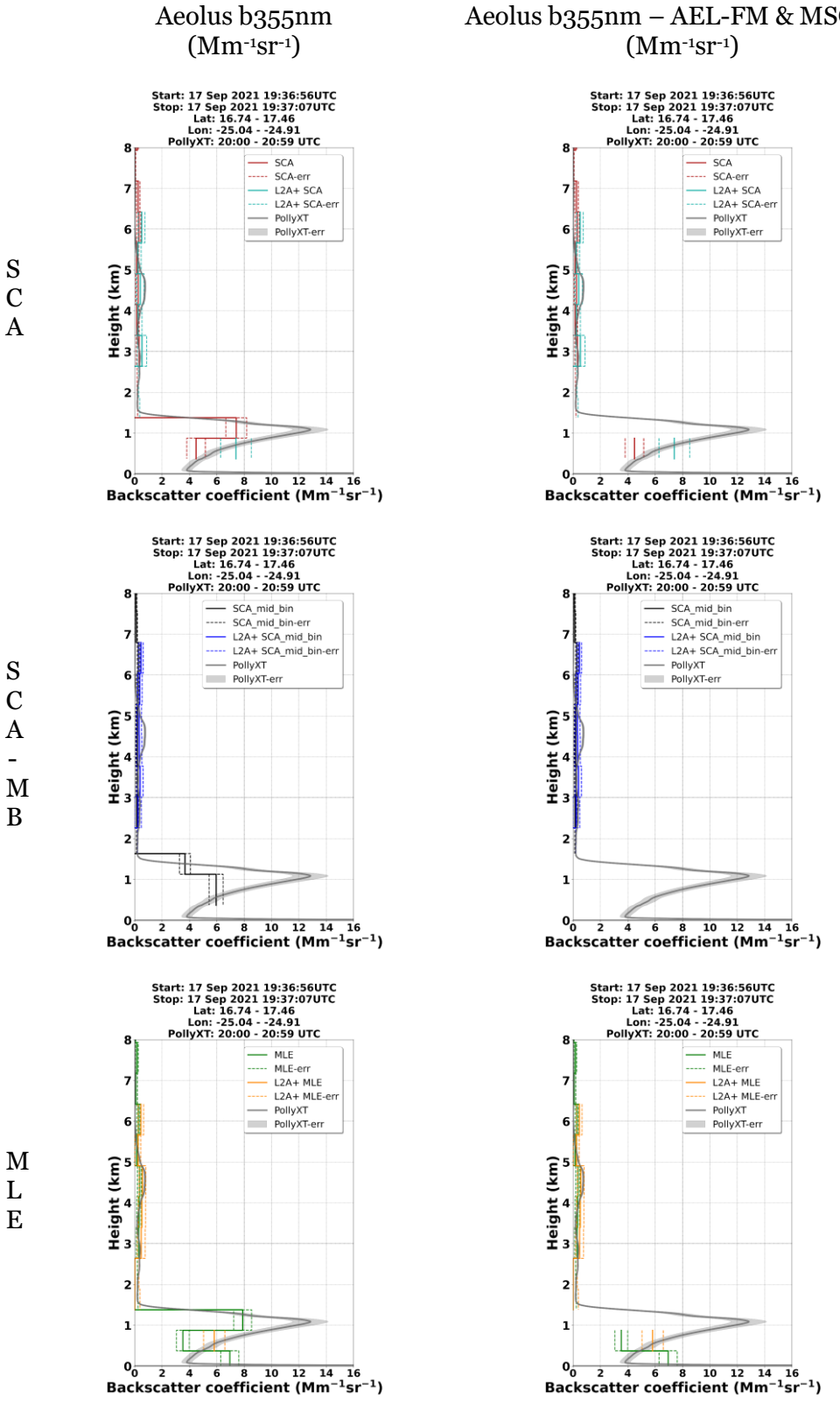

Figure 5.15: Vertical profiles of the raw Aeolus L2A and QA L2A+ backscatter coefficient at 355 nm retrieved from the SCA, SCA mid-bin and MLE algorithms with the corresponding backscatter

profiles at 532 nm acquired by PollyXT ground-based lidar (left panel), and QA Aeolus L2A and L2A+ backscatter profiles for the SCA, SCA mid-bin and MLE algorithms with the derived backscatter profiles from PollyXT lidar (right panel).

5.3. The case of the 24th of September 2021.

5.3.1. Description of the atmospheric scene.

For the third study case on 24th September 2021, Figure 5.16 presents the ALADIN's measurement track (id 017901), the spatial distribution of the "clear" and 'cloudy' areas on a pixel level derived from the MSG-SEVIRI CLAAS-3 cloud dataset, the AEL-FM feature mask product retrieved for the specific atmospheric scene and the transformed AEL-FM product to the Aeolus BRC scale giving the cloud-fraction (in %) of each BRC profile. According to the AEL-FM product, an area with strong returns mostly attributed the presence of clouds can be detected between the latitudes 33° and 45°N and altitudes between 5 and 14km with the lidar beam being fully attenuated below 5km.

Aeolis Orbit

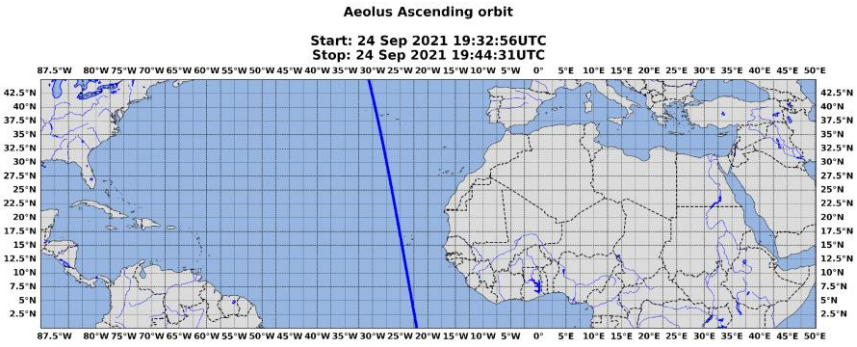

MSG Cloud Coverage

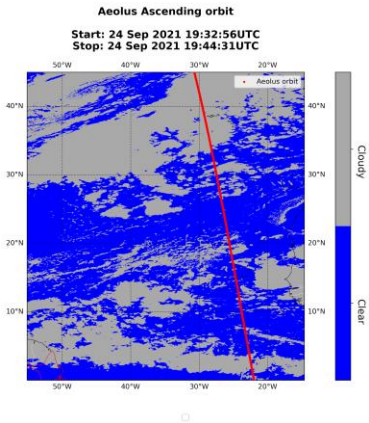

AEL-FM

RAW

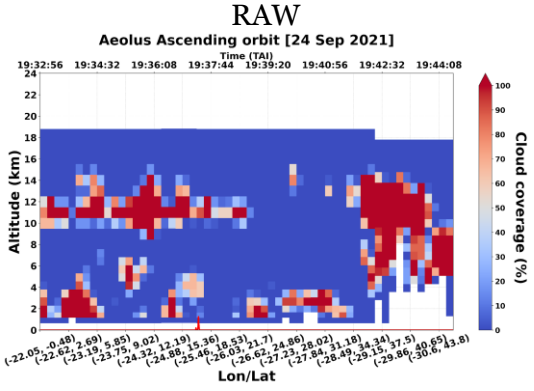

MID

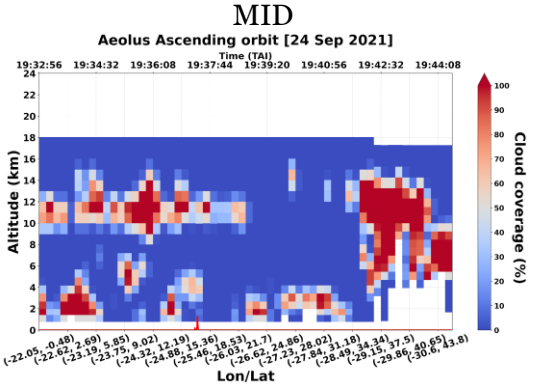

F
M

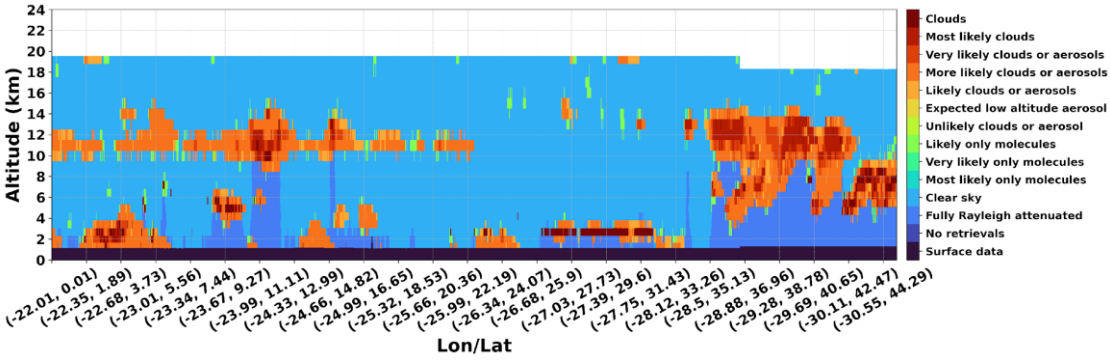

Figure 5.16: Aeolus ascending orbit (id: 017901) over the L2A+ RoI on 24th September 2021 and the time-closest spatial distribution of "cloudy" and "clear" pixels derived from the binary cloud-mask product of MSG-SEVIRI CLAAS-3 dataset (upper panel). The transformed AEL-FM product to the Aeolus BRC scale for the regular (24 bins) and middle-bin vertical scale (23 bins) (middle panel) and the AEL-FM feature mask product at the Aeolus measurement scale (~3km horizontal resolution) with the classified features of the probed atmospheric scene.

In Figure 5.17, the vertically resolved profiles of dust mass concentration from CAMS along the Aeolus orbit (id: 017901) are depicted for each vertical scale (regular vertical scale with 24 bins and middle-bin scale with 23 bins). The vertical profiles of dust fraction (in %) along the Aeolus measurement track are also depicted in Figures 5.17b, and d. According to the dust profiles, an identified dust layer covers the latitudinal band between 5° and 17°N and up to 4km with elevated dust mass concentration and dust fraction values.

Dust Mass Concentration (μg/m3)

Dust Percentage (%)

R
A
W

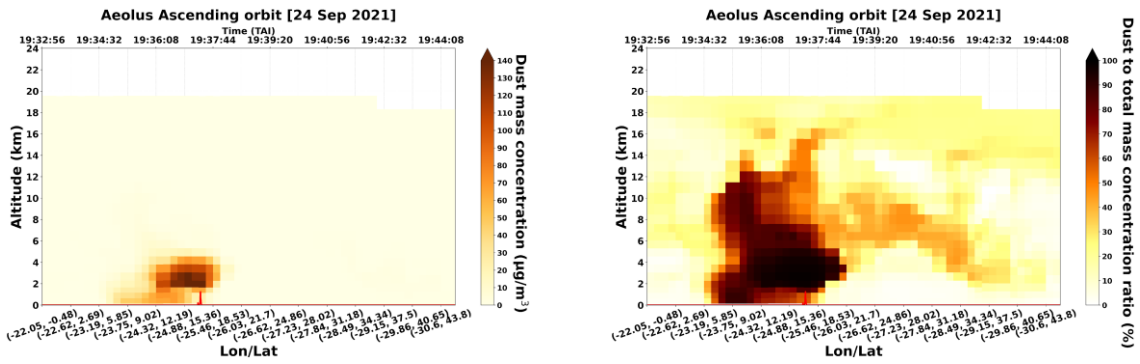

M
I
D

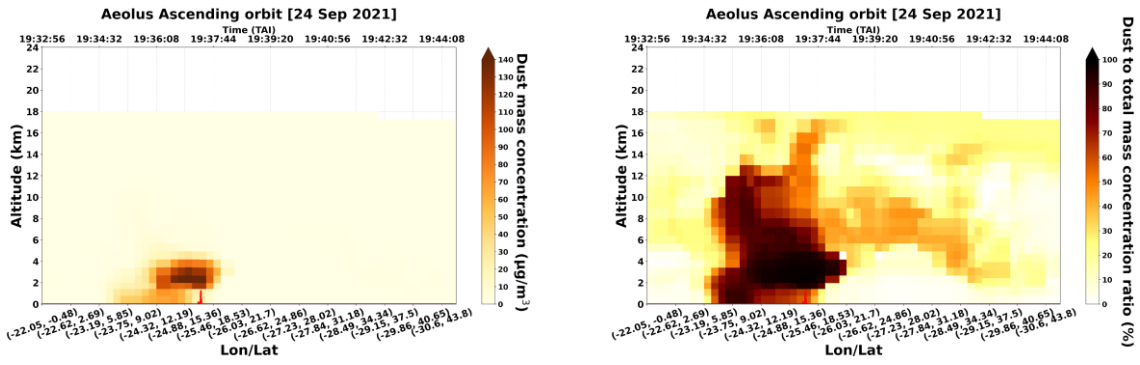

Figure 5.17: Vertical profiles of CAMS dust mass concentration and dust-to-total aerosol mass concentration ratio along the Aeolus orbit (id: 017901) provided at the regular (a, b) and middle-bin (c, d) vertical scales for the study case on the 24th of September 2021.

5.3.2. Aeolus Optical Products.

Below, we present the vertical profiles of the unprocessed (left panel) and QA (right panel) pure-aerosol Aeolus L2A retrievals of the co-polar backscatter coefficient at 355 nm along the Aeolus overpass (id 017901) for the three L2A retrieval algorithms of SCA, SCA mid-bin and MLE.

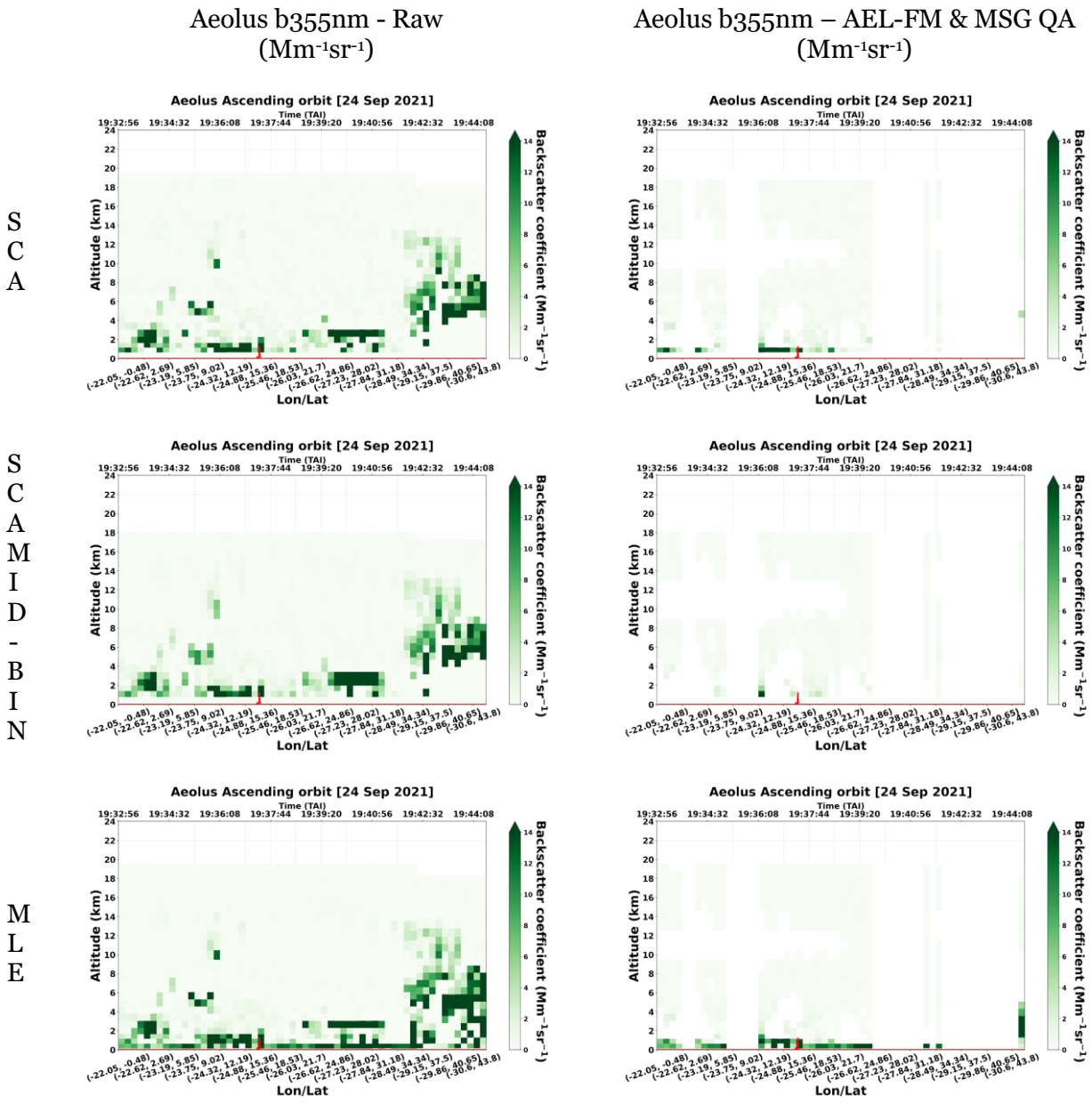

Figure 5.18 Raw Aeolus L2A backscatter profiles at 355 nm along the Aeolus orbit (id 017901) retrieved from the SCA, SCA mid-bin and MLE algorithms (left panel) and the corresponding QA

pure-aerosol backscatter profiles at 355 nm for the SCA, SCA mid-bin and MLE algorithms (right panel).

5.3.3. L2A and L2A+ products.

Figure 5.19 illustrates for the given study case the pure-dust Aeolus co-polar backscatter profiles at 355 nm produced with the SCA and SCA mid-bin algorithms and the associated missing cross-polar backscatter component for each profile along the Aeolus overpass. It can be noticed the significantly lower number of BRC bins after the implementation of the filtering tools.

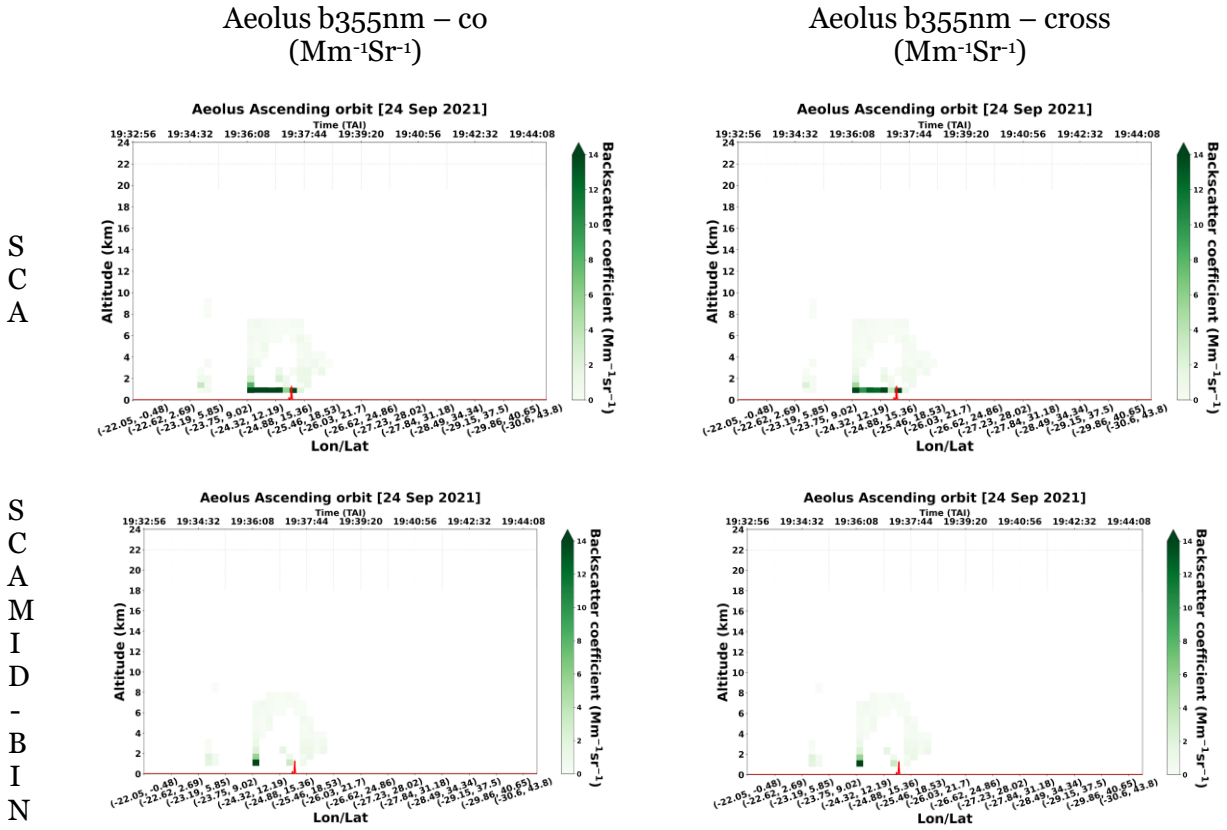

Figure 5.19: Co-polar and cross polar backscatter profiles along the Aeolus overpass (id 017901) for the SCA (a, b) and SCA mid-bin algorithms (c, d).

5.3.4. L2A+ - ESA-eVe validation.

The current section deals with the intercomparison of the new Aeolus product (L2A+) against ground-based retrievals from eVe lidar for the third study case on 24th of September 2021 (orbit id: 017901). The comparison process of the raw Aeolus L2A and QA L2A+ retrievals of the co-polar and total backscatter coefficient at 355 nm respectively with the backscatter profile at 355 nm from eVe lidar is illustrated on the left panel of Figure 5.20 while on the right panel the same comparison process is presented taking into account the QA Aeolus L2A backscatter. According to our results, in the case of all the L2A retrieval algorithms including the SCA, SCA mid-bin, and MLE algorithms, the misdetection of the cross-polar component of the backscattered signal worsens the agreement

between Aeolus and ground-based eVe system with the former presenting an underestimation in the values of backscatter coefficient. On the contrary, within the available height range of comparison, a very good agreement with a slight underestimation in the backscatter coefficient is pointed out of the improved Aeolus L2A+ product retrieved from the SCA algorithm compared with the backscatter coefficient from eVe lidar. We similarly notice a very good agreement between the L2A+ backscatter profile at 355 nm retrieved from the MLE algorithm and the corresponding profile from the ground-based system especially within the lowermost identified dust layer with quite similarly backscatter coefficient values between the two systems ranging from 10 to 13 $Mm^{-1}sr^{-1}$. Regarding the SCA mid-bin algorithm for the specific study case, both L2A and L2A+ show an underestimation in the retrieved backscatter coefficient values compared with the eVe backscatter retrievals in the available Aeolus bins.

Aeolus b355nm ($Mm^{-1}sr^{-1}$)

Aeolus b355nm – AEL-FM & MSG QA ($Mm^{-1}sr^{-1}$)

SCA

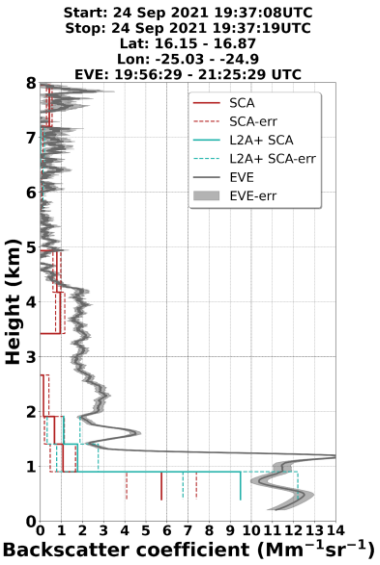

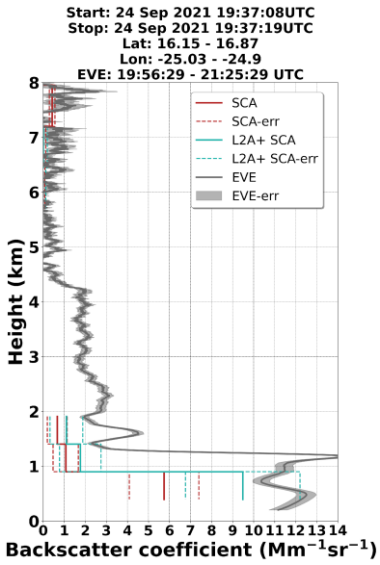

SCA-MB

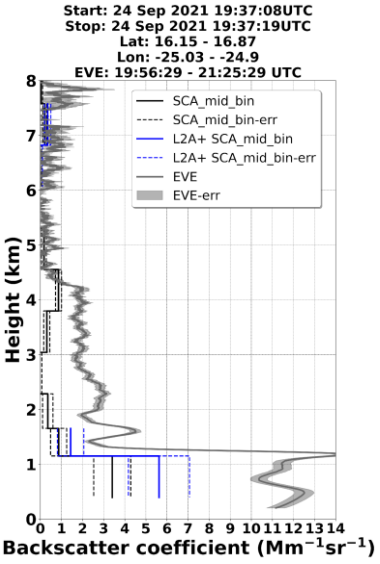

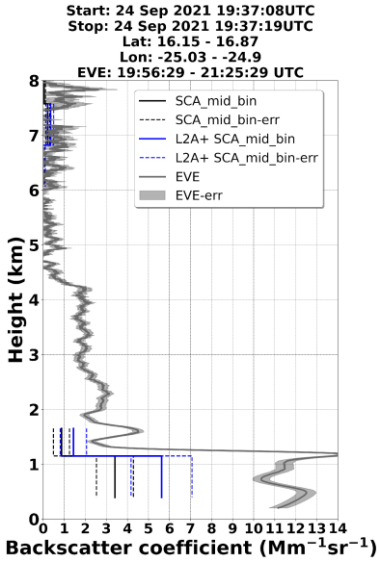

M
L
E

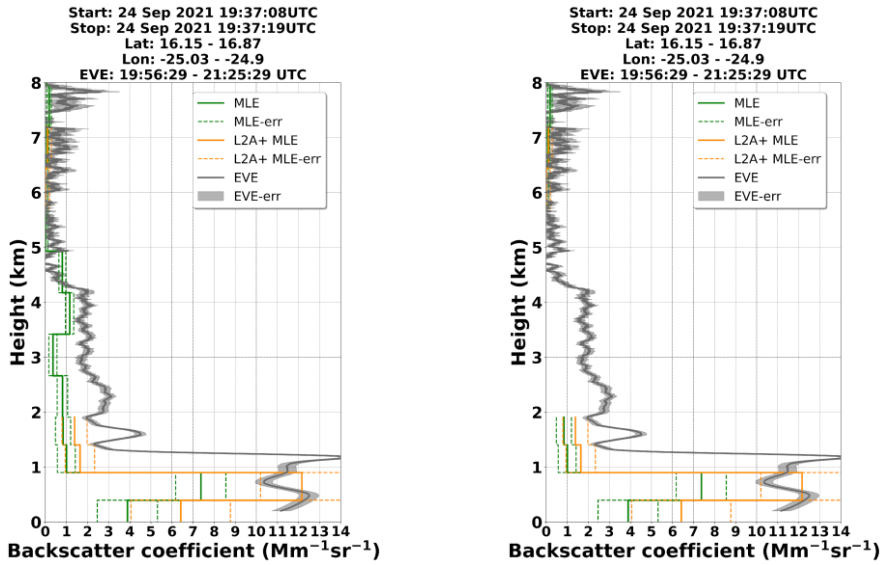

Figure 5.20: Vertical profiles of the raw Aeolus L2A and QA L2A+ backscatter coefficient at 355 nm retrieved from the SCA, SCA mid-bin and MLE algorithms with the corresponding backscatter profiles at 355 nm acquired by eVe ground-based lidar (left panel), and QA Aeolus L2A and L2A+ backscatter profiles for the SCA, SCA mid-bin and MLE algorithms with the derived backscatter profiles from eVe lidar (right panel). Study case 24 September 2021.

5.3.5. L2A+ - ESA-PollyXT validation.

In the current section, the comparison of the Aeolus L2A and L2A+ backscatter coefficient for the three retrieval algorithms (SCA, SCA mid-bin and MLE) against the ground-based retrieved backscatter coefficient from PollyXT is presented for the third study case on 24 September 2021 in Figure 5.21. The results show an improvement with a slight underestimation of the L2A+ SCA mid-bin backscatter coefficient compared against the acquired backscatter coefficient from PollyXT lidar. Regarding the retrieved L2A+ backscatter profiles from the SCA and MLE algorithms, the correction of the backscattered lidar signal results in an overestimation in the backscatter coefficient up to 1km when compared with the PollyXT backscatter values at 532 nm. On the contrary, above the altitude of 1km an underestimation of the L2A+ backscatter coefficient is pointed out for both retrieval algorithms compared with the PollyXT backscatter values.

	Aeolus b355nm ($Mm^{-1}sr^{-1}$)	Aeolus b355nm – AEL-FM & MSG QA ($Mm^{-1}sr^{-1}$)
SCA	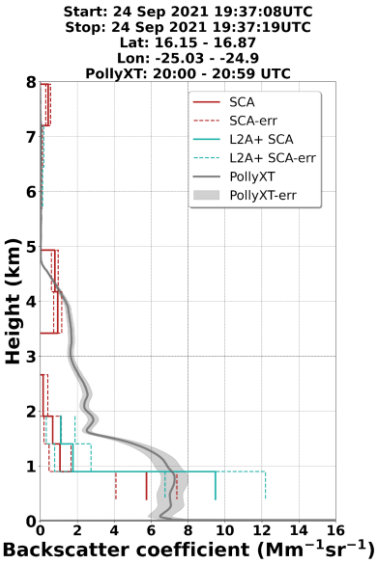	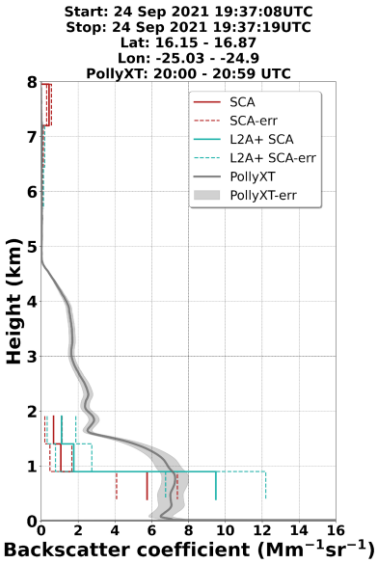
SCA-MB	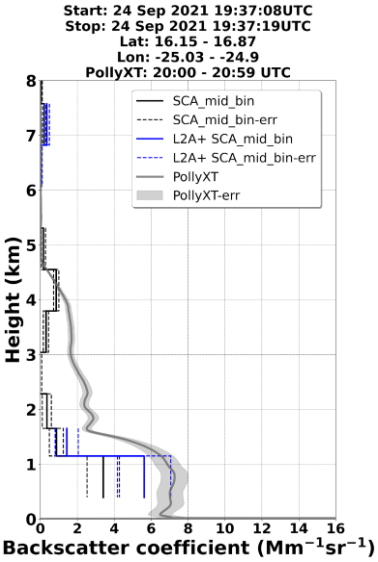	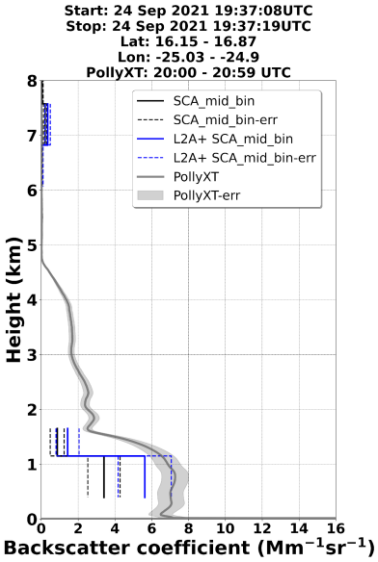

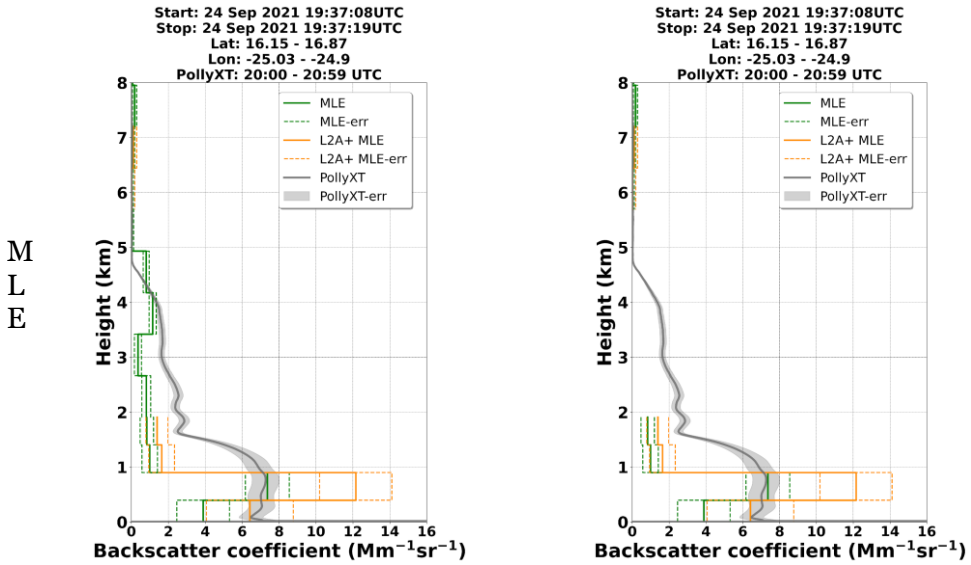

Figure 5.21: Vertical profiles of the raw Aeolus L2A and QA L2A+ backscatter coefficient at 355 nm retrieved from the SCA, SCA mid-bin and MLE algorithms with the corresponding backscatter profiles at 532 nm acquired by PollyXT ground-based lidar (left panel), and QA Aeolus L2A and L2A+ backscatter profiles for the SCA, SCA mid-bin and MLE algorithms with the derived backscatter profiles from PollyXT lidar (right panel).

5.4. Overall assessment of the L2A/L2A+ Aeolus product

An overall assessment of the original (L2A) and corrected (L2A+) Aeolus SCA, SCA mid-bin, and MLE pure-dust backscatter retrievals was also performed using reference ground-based measurements from the eVe and PollyXT lidars operated during the ASKOS experiment at Mindelo, Cape Verde and specifically during July and September 2021, and during June and September 2022. The main aim of this assessment analysis was to check how well the refined Aeolus L2A+ dust product performs when compared with the ground-based retrievals. For this comparison process, we used all the collocated backscatter profiles of the ground-based reference lidars with Aeolus, with spatial and temporal differences lower than 40 km and 2h respectively. Moreover, for the sake of comparison, the ground-based eVe and PollyXT profiles have been rescaled to match Aeolus vertical resolution. This was performed by averaging values of all the ground-based retrievals, residing within the altitude margins of each Aeolus BRC for the Aeolus regular vertical scale (24 bins) and the middle bin vertical scale (23 bins). Following the aforementioned collocation criteria, we found 14 Aeolus-eVe and 10 Aeolus-PollyXT profile coincidences available for comparison with the SCA, SCA-MB and MLE products.

The final dataset of Aeolus vs eVe pure-dust backscatter coefficients for the 4-month period is presented in Figure 5.22 for the original (L2A) Aeolus retrievals (left) and the corrected (L2A+) product (right) after the adjustment of the missing cross-polar backscatter component. In addition, the scatter plot comparison is illustrated separately for the Aeolus SCA (upper panel), MLE (middle panel), and SCA mid-bin (lower panel) retrieval algorithms. The associated evaluation scores are summarized in Table 1. It is worth reminding that the available number of Aeolus-eVe matched pairs has been significantly reduced due to the implemented cloud-filtering and dust-typing approaches. Note that we have also eliminated all the Aeolus-eVe pairs in which the SCA, SCA mid-bin, and MLE backscatter coefficients exceed the value of 20 Mm^{-1} sr^{-1} in order to avoid possible contamination of extreme outliers in the calculated metrics in cases when incorrectly, a presence of clouds has not

been detected and eliminated by the cloud-filtering approaches. The regression linear fit equation in Figure 5.22 gives us information regarding the relationship between the satellite and ground-based backscatter retrievals. Specifically, the slope of the linear regression line indicates how close the satellite-retrieved backscatter coefficient is with regard to ground-based backscatter retrievals and intercept provides the associated error. Deviations from these values show biases in the retrieved backscatter coefficient by Aeolus. Extra information regarding the relationship of both satellite and ground-based backscatter retrievals can be derived by the Pearson correlation coefficient (R), the root mean square error (RMSE) and the mean absolute bias. All the aforementioned statistical metrics have been calculated and are presented in Table 1. According to our results, for the L2A Aeolus product, we found significant biases (absolute difference of the means: averaged Aeolus backscatter minus the averaged eVe backscatter) of the order of -0.34 Mm-1 sr-1 for SCA and MLE algorithms, and -0.39 Mm-1sr-1 for the SCA-MB with RMSE values ranging from 1.04 Mm-1sr-1 for SCA-MB to 1.48 Mm-1sr-1 for SCA. The negative absolute biases reveal that the original Aeolus (L2A) product underestimates the backscatter coefficient when dust particles are probed by ALADIN due the missing cross-polar component of the backscattered lidar signal. Moreover, Pearson correlation coefficients of the order of 0.56 and 0.57 for the SCA, and SCA-MB retrieval algorithms respectively, reveal a fairly good agreement for both collocated datasets. For the MLE algorithm, a lower correlation coefficient value of the order of 0.48 has been recorded which also reveals a quite good agreement for Aeolus-eVe datasets. Referring to the L2A+ Aeolus product comparison, the results reveal that while Pearson's correlation coefficient remains constant for both L2A and L2A+ products, the adjustment of the missing cross-polar component in the retrieved backscatter coefficients significantly improves the slope of the linear regression from 0.56 (L2A) to 0.93 (L2A+) for the SCA-MB backscatter retrievals and from 0.51 (L2A) to 0.84 (L2A+) for the MLE retrievals. A significant improvement is also pointed out in the retrieved mean absolute bias score for all the retrieval algorithms. To be more specific, for the SCA-MB algorithm, the absolute bias score between Aeolus L2A+ and eVe backscatters is down to 0.05 Mm-1sr-1 from -0.39 Mm-1sr-1 for the original L2A product. Improvements in the retrieved mean absolute biases are also observed for the SCA and MLE algorithms with values falling from -0.34 at 0.1 Mm-1sr-1 for the L2A+ product. However, these improvements in the absolute bias scores are accompanied by an increase in the retrieved RMSEs for all the applied algorithms especially for the SCA which reaches the 2.33 Mm-1sr-1 from 1.48 Mm-1sr-1 (see Table 2).

a)

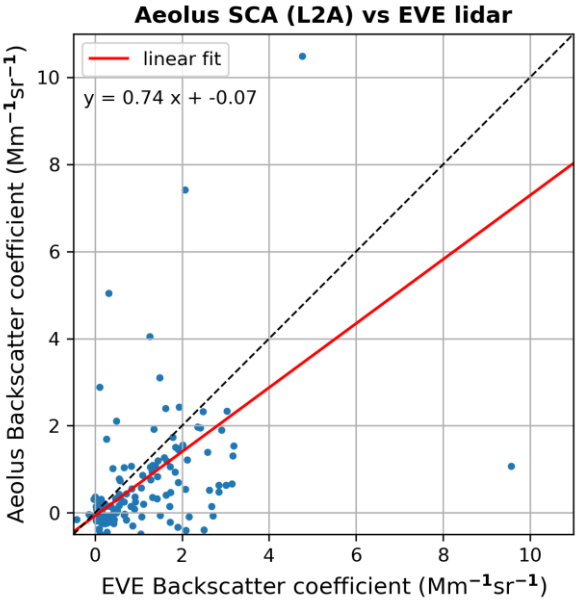
Aeolus SCA (L2A) vs EVE lidar
linear fit
y = 0.74 x + -0.07
Aeolus Backscatter coefficient (Mm⁻¹sr⁻¹)
EVE Backscatter coefficient (Mm⁻¹sr⁻¹)

b)

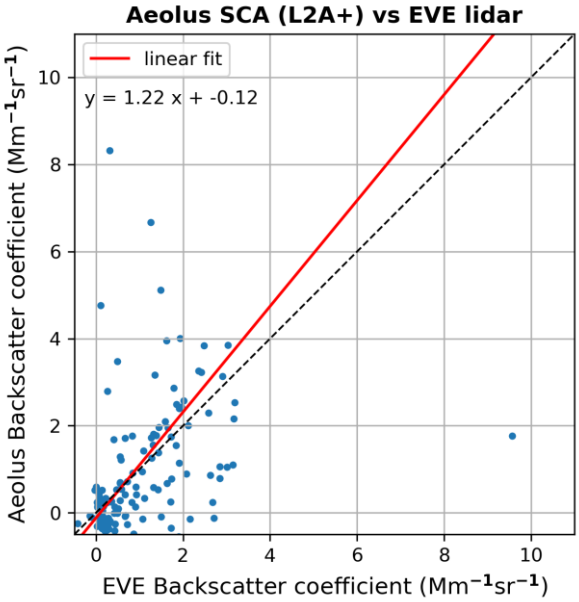
Aeolus SCA (L2A+) vs EVE lidar
linear fit
y = 1.22 x + -0.12
Aeolus Backscatter coefficient (Mm⁻¹sr⁻¹)
EVE Backscatter coefficient (Mm⁻¹sr⁻¹)

c)

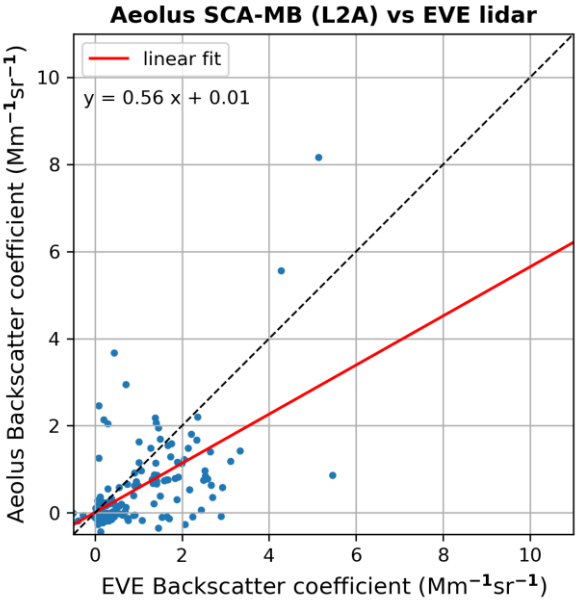
Aeolus SCA-MB (L2A) vs EVE lidar
linear fit
y = 0.56 x + 0.01
Aeolus Backscatter coefficient (Mm⁻¹sr⁻¹)
EVE Backscatter coefficient (Mm⁻¹sr⁻¹)

d)

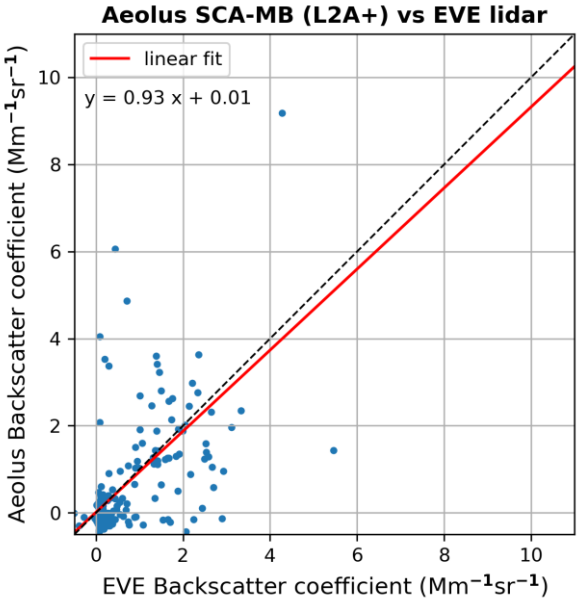
Aeolus SCA-MB (L2A+) vs EVE lidar
linear fit
y = 0.93 x + 0.01
Aeolus Backscatter coefficient (Mm⁻¹sr⁻¹)
EVE Backscatter coefficient (Mm⁻¹sr⁻¹)

e) f)

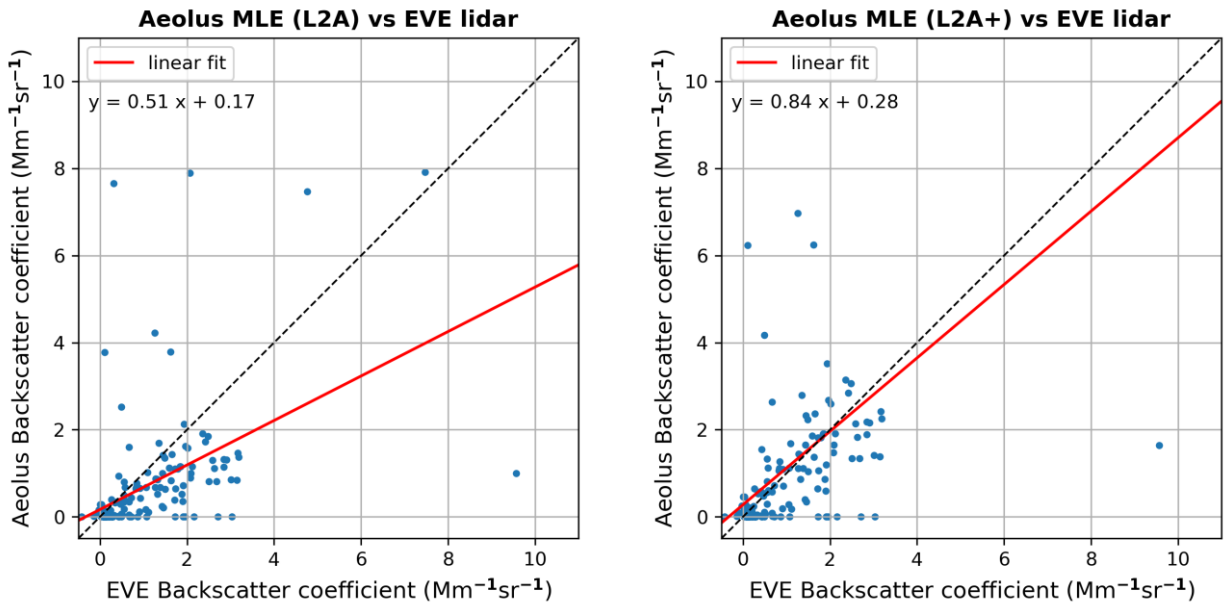

Figure 5.22. Scatterplot comparison between Aeolus (in y axis) and eVe ground-based (in x axis) backscatter coefficient retrievals during the 4-month period of eVe/ASKOS operations at Cape Verde/Mindelo station. In the left and right panels, the results for the original (L2A) and corrected (L2A+) Aeolus retrievals are presented respectively and separately for the SCA (a, b), SCA-MB (c,d), and MLE (e,f) applied algorithms.

Algo	**L2A**						**L2A+**					
	N	**Slope**	**Intercept**	**B_a**	**RMSE**	**R**	**N**	**Slope**	**Intercept**	**B_a**	**RMSE**	**R**
SCA	154	0.74	-0.07	-0.34	1.48	0.56	154	1.22	-0.12	0.1	2.33	0.56
SCA-MB	155	0.56	0.01	-0.39	1.04	0.57	155	0.93	0.01	0.05	1.4	0.57
MLE	157	0.51	0.17	-0.34	1.38	0.48	157	0.84	0.28	0.1	1.96	0.48

Table 1. Statistical indicators acquired from the comparison of the Aeolus L2A/L2A+ backscatter retrievals (in Mm-1sr-1) with ground-based observations from eVe lidar during the 4-month period of ASKOS experiment at Cape Verde/Mindelo station. The following statistical parameters are included: total number of matched Aeolus-eVe pairs (N), mean absolute bias (Ba), root-mean-square error (RMSE), and correlation coefficient R.

The scatter plot comparisons between Aeolus L2A/L2A+ and PollyXT backscatter retrievals and separately for each of the three applied algorithms are illustrated in Figure 5.23. The associated evaluation scores are summarized in Table 3 for the Aeolus L2A and L2A+ products respectively. Compared with the Aeolus-eVe dataset, in this case, we can observe that the available number of the collocated Aeolus-PollyXT backscatter measurements is lower due to the shorter operation period of the ground-based PollyXT lidar (3 months). Focusing on the left panel of Fig. 5.23 which illustrates the comparison between the Aeolus L2A and ground-based backscatter retrievals, it is evident that as in the case of Aeolus-eVe comparison, the satellite underestimates the backscatter coefficient for all the applied algorithms. The slope of the linear regression between the two datasets ranges from 0.31 for the MLE to 0.43 for the SCA-MB and has a Pearson correlation coefficient for both comparisons of the order of 0.4 and 0.57 respectively. After the adjustment of the missing cross-polar backscatter component in the L2A+ retrievals (Fig. 5.23, right panel), the regression slopes for the three applied algorithms show better agreement with the ground-truth reaching the values of 0.66 for the SCA, 0.71 for the SCA-MB, and 0.52 for the MLE. Moreover, absolute biases between Aeolus and PollyXT backscatter coefficients are down to -0.01 Mm-1sr-1 from -0.17 Mm-1sr-1 for the SCA, while for the SCA-MB, and MLE algorithms the absolute biases reach the values of -0.03 and -0.02 Mm-1sr-1 from -0.3 and -0.36 Mm-1sr-1 respectively. Nevertheless, the obtained improvements on bias scores for the Aeolus L2A+ backscatter retrievals are not accompanied by reductive tendencies on RMSE levels. On the contrary, they show an increase of about ~36% and ~ 24% for the SCA and MLE reaching the values of 2.39 and 2.06 Mm-1sr-1 respectively, while a lower increase of the order of ~21% is recorded for the SCA-MB algorithm reaching the value of 1.39 Mm-1sr-1.

a) b)

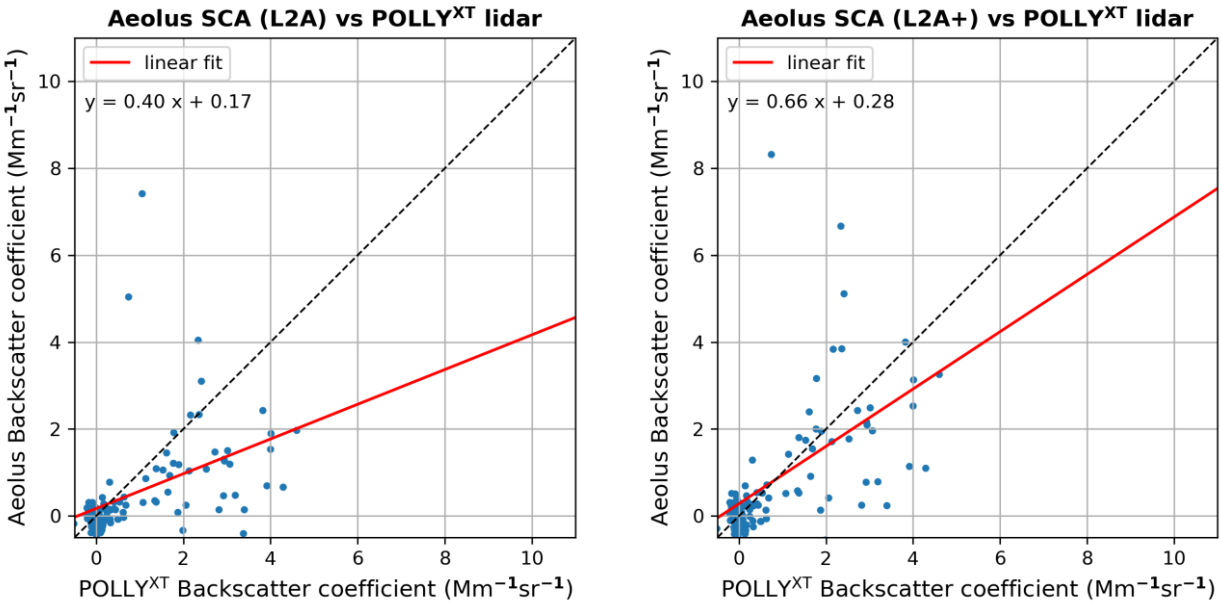

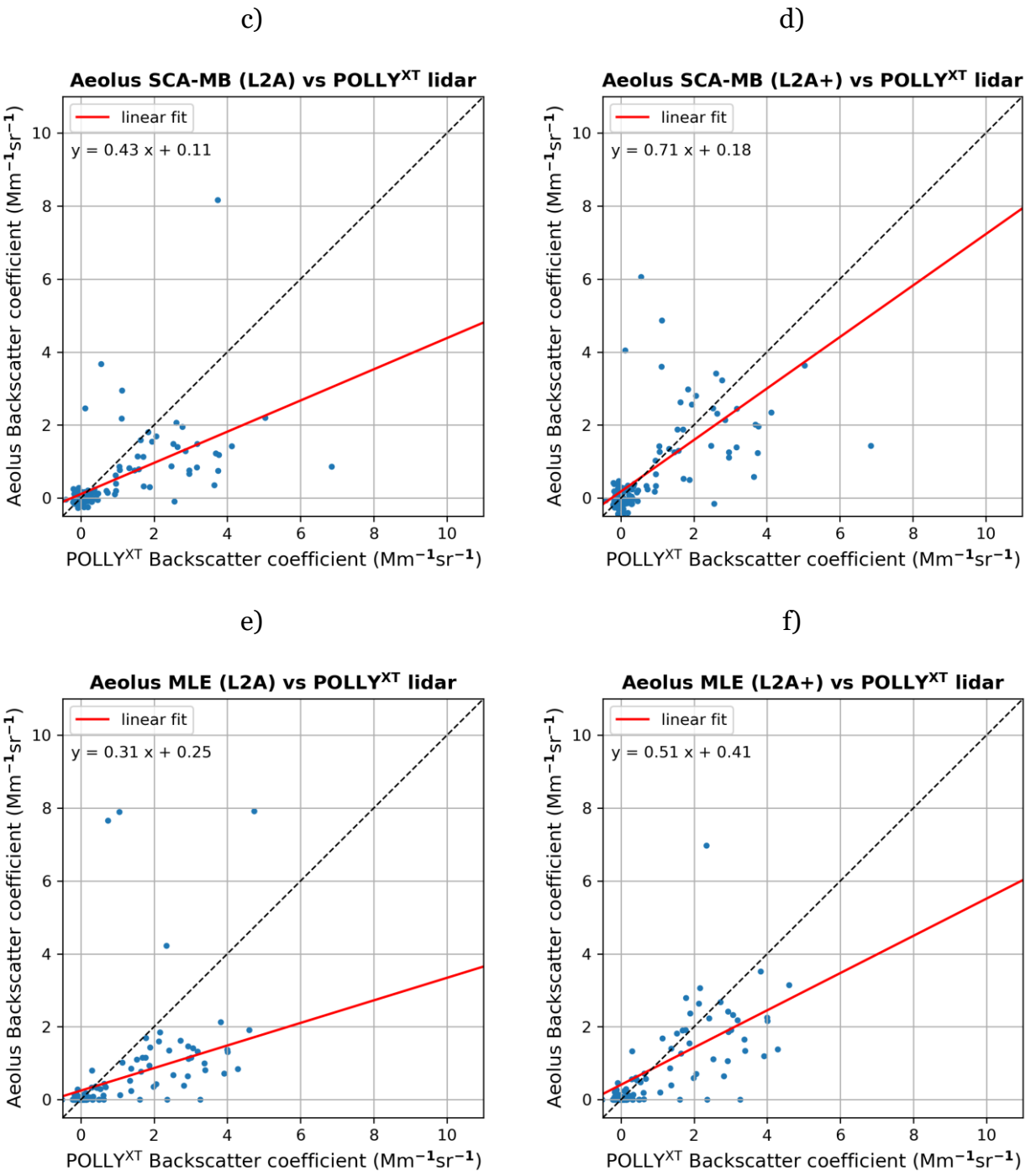

Figure 5.23. Scatterplot results same as in Figure 5.22 but for the comparison between the Aeolus L2A/L2A+ backscatter retrievals with observations from PollyXT ground-based lidar.

Algo	L2A						L2A+					
	N	**Slope**	**Intercept**	**B_a**	**RMSE**	**R**	**N**	**Slope**	**Intercept**	**B_a**	**RMSE**	**R**
SCA	135	0.4	0.17	-0.34	1.75	0.42	135	0.66	0.28	-0.01	2.39	0.42
SCA-MB	131	0.43	0.11	-0.3	1.14	0.57	131	0.71	0.18	-0.03	1.39	0.57
MLE	136	0.31	0.25	-0.36	1.65	0.4	136	0.51	0.41	-0.02	2.06	0.4

Table 2. As in Table 1 but for the comparison between the Aeolus L2A/L2A+ backscatter retrievals (in Mm-1sr-1) with ground-based observations from the PollyXT lidar during the ASKOS experiment.

To conclude, the overall comparison between the Aeolus vs eVe and Aeolus vs PollyXT backscatter retrievals over the detected dust layers and during the entire period of ASKOS operation at Cabo Verde/ Mindelo station, reveals a noteworthy improvement in the agreement between satellite and ground-based observations in the case of the corrected L2A+ backscatter estimates. The agreement is more pronounced between Aeolus and ground-based eVe lidar and especially for the SCA-MB, and MLE retrieval algorithms, converging towards the ideal evaluation scores in the case of the L2A+ product.

6. Conclusions

Towards overcoming the inherent weakness of the Aeolus' lidar system (ALADIN) attributed to the missing cross-polar component of the atmospheric backscattered returns of the circularly polarized emitted beam, the L2A+ study develops an improved Aeolus product. Towards this objective, the study aims to implement the novel L2A+ product on aerosol assimilation towards improved dust transport modelling and for further enhancing NWP.

The development of the new product utilized a synergy of processing tools including the Aeolus Feature Mask product (AEL-FM) and the MSG CLAAS-3 cloud dataset from SEVIRI for cloud screening as well as reanalysis numerical outputs produced by the Copernicus Atmosphere Monitoring Service (CAMS). The study period refers to the period of the ASKOS experiment at Mindelo, Cape Verde and specifically during July and September 2021, and during June and September 2022. The region of interest refers to an extended domain including the Sahara Desert and the Tropical Atlantic Ocean up to the Caribbean Sea.

For the evaluation and validation of the L2A+ product, the available dataset from the ASKOS campaign was used. In the current section, the results of our analysis were presented for three indicative Aeolus overpasses over Mindelo, Cabo Verde on the 10th, 17th, and 24th of September 2021 and include among others the raw Aeolus L2A retrievals retrieved from the Standard Correct Algorithm (SCA), the SCA mid-bin and MLE algorithms, and the quality-assured Aeolus L2A retrievals after the implementation of all the available filtering tools. The focus was given on the pure-dust Aeolus L2A+ total backscatter at 355 nm, the extinction coefficient at 355 nm and the final dust mass concentration product. The assessment analysis of the satellite L2A and L2A+ retrievals versus the corresponding measurements obtained from eVe and PollyXT lidars was examined under three study cases on 10, 17, and 24 September. The results for the three cases reveal an underestimation of the L2A particle backscatter coefficient retrieved from the three algorithms (SCA, SCA mid-bin and MLE) compared to the ground-based systems. This underestimation which has already been demonstrated in previous studies is mostly connected to the misdetection of the cross-polar backscatter component when non-spherical mineral particles are recorded. In the case of the enhanced Aeolus product (L2A+), the results for the three study cases reveal that the discrepancies between the retrieved satellites and ground-based backscatter retrievals are reduced in most cases enhancing our expectations about the ability of the new Aeolus product to provide valuable information on the detection and characterization of significant aerosol layers. Especially the retrieved backscatter profiles from the MLE algorithm present a satisfactory agreement with the corresponding profiles from eVe and PollyXT lidars throughout the greatest part of the detected dust layers.

Towards achieving a more robust statistical analysis, our dataset was extended in time in order to obtain an increased number of collocated and concurrent Aeolus and ground-based cases. Specifically, the WP2000 outcomes and the available Aeolus dataset processed with Baseline 16 were enriched with additional measurements acquired from the ASKOS operations at Mindelo, Cape Verde during July/September 2021, and June/September 2022. The overall comparison between Aeolus and eVe ground-based measurements revealed that the adjustment of the missing cross-polar component in the retrieved co-polar backscatter coefficient resulted in a significant improvement of the satellite product performance. Specifically, among the three applied algorithms (SCA, SCA Mid-bin, MLE) presented here, a better improvement was found for the SCA Mid-bin and MLE algorithms, compared with the SCA algorithm. Regarding the Aeolus-PollyXT comparison for the three applied algorithms, the results reveal an improvement in the agreement between the Aeolus L2A+ and ground-based retrievals. However, the computed evaluation metrics do not provide strong evidence of which of the three algorithms performs better.

The agreement presented here between the enhanced Aeolus L2A+ dust product and the ground-based retrievals makes the new Aeolus dataset an ideal candidate to be implemented on aerosol assimilation towards improving dust transport modeling and for further enhancing the NWP. Moreover, the expansion of the L2A+ product development in terms of time and space will facilitate and hopefully encourage accurate, climatological dust studies in a global scale.

List of Figures

	(left panel), and QA Aeolus L2A and L2A+ backscatter profiles for the SCA, SCA mid-bin and MLE algorithms with the derived backscatter profiles from eVe lidar (right panel).
Figure 5.8	Vertical profiles of the raw Aeolus L2A and QA L2A+ backscatter coefficient at 355 nm retrieved from the SCA, SCA mid-bin and MLE algorithms with the corresponding backscatter profiles at 355 nm acquired by PollyXT ground-based lidar (left panel), and QA Aeolus L2A and L2A+ backscatter profiles for the SCA, SCA mid-bin and MLE algorithms with the derived backscatter profiles from PollyXT lidar (right panel).
Figure 5.9	Aeolus ascending orbit (id: 017790) over the L2A+ RoI on 17th September 2021 and the time-closest spatial distribution of "cloudy" and "clear" pixels derived from the binary cloud-mask product of MSG-SEVIRI CLAAS-3 dataset (upper panel). The transformed AEL-FM product to the Aeolus BRC scale for the regular (24 bins) and middle-bin vertical scale (23 bins) (middle panel) and the AEL-FM feature mask product at the Aeolus measurement scale (~3km horizontal resolution) with the classified features of the probed atmospheric scene.
Figure 5.10	Vertical profiles of CAMS dust mass concentration and dust-to-total aerosol mass concentration ratio along the Aeolus orbit (id: 017790) provided at the regular (a, b) and middle-bin (c, d) vertical scales for the study case on the 17th of September 2021.
Figure 5.11	(a) CALIPSO total backscatter coefficient at 532 nm. (b) CALIPSO particulate depolarization ratio at 532 nm (c) CALIPSO QA pure-aerosol total backscatter coefficient at 532 nm (d) CALIPSO QA pure-dust backscatter coefficient at 532 nm. Study case: 17th September 2021.
Figure 5.12	Raw Aeolus L2A backscatter profiles at 355 nm along the Aeolus orbit (id 017790) retrieved from the SCA, SCA mid-bin and MLE algorithms (left panel) and the corresponding QA pure-aerosol backscatter profiles at 355 nm for the SCA, SCA mid-bin and MLE algorithms (right panel).
Figure 5.13	Co-polar and cross polar backscatter profiles along the Aeolus overpass (id 017790) for the SCA (a, b) and SCA mid-bin algorithms (c, d).
Figure 5.14	Vertical profiles of the raw Aeolus L2A and QA L2A+ backscatter coefficient at 355 nm retrieved from the SCA, SCA mid-bin and MLE algorithms with the corresponding backscatter profiles at 355 nm acquired by eVe ground-based lidar (left panel), and QA Aeolus L2A and L2A+ backscatter profiles for the SCA, SCA mid-bin and MLE algorithms with the derived backscatter profiles from eVe lidar (right panel).
Figure 5.15	Vertical profiles of the raw Aeolus L2A and QA L2A+ backscatter coefficient at 355 nm retrieved from the SCA, SCA mid-bin and MLE algorithms with the corresponding backscatter profiles at 532 nm acquired by PollyXT ground-based lidar (left panel), and QA Aeolus L2A and L2A+ backscatter profiles for the SCA, SCA mid-bin and MLE algorithms with the derived backscatter profiles from PollyXT lidar (right panel).
Figure 5.16	Aeolus ascending orbit (id: 017901) over the L2A+ RoI on 24th September 2021 and the time-closest spatial distribution of "cloudy" and "clear" pixels derived from the binary cloud-mask product of MSG-SEVIRI CLAAS-3 dataset (upper panel). The transformed AEL-FM product to the Aeolus BRC scale for the regular (24 bins) and middle-bin vertical scale (23 bins) (middle panel) and the AEL-FM feature mask product at the Aeolus measurement scale (~3km horizontal resolution) with the classified features of the probed atmospheric scene.
Figure 5.17	Vertical profiles of CAMS dust mass concentration and dust-to-total aerosol mass concentration ratio along the Aeolus orbit (id: 017901) provided at the regular (a,

List of Tables

[End of ESA-L2A+ DI04]